© 2020. Published by The Company of Biologists Ltd | Journal of Experimental Biology (2020) 223, jeb215905. doi:10.1242/jeb.215905

RESEARCH ARTICLE

The brains of six African mole-rat species show divergent responses to hypoxia

Samantha M. Logan[1,*], Kama E. Szereszewski[1,*], Nigel C. Bennett[2], Daniel W. Hart[2], Barry van Jaarsveld[2], Matthew E. Pamenter[3,4] and Kenneth B. Storey[1,‡]

ABSTRACT

Mole-rats are champions of self-preservation, with increased longevity compared with other rodents their size, strong antioxidant capabilities and specialized defenses against endogenous oxidative stress. However, how the brains of these subterranean mammals handle acute *in vivo* hypoxia is poorly understood. This study is the first to examine the molecular response to low oxygen in six different species of hypoxia-tolerant mole-rats from sub-Saharan Africa. Protein carbonylation, a known marker of DNA damage (hydroxy-2′-deoxyguanosine), and antioxidant capacity did not change following hypoxia but HIF-1 protein levels increased significantly in the brains of two species. Nearly 30 miRNAs known to play roles in hypoxia tolerance were differentially regulated in a species-specific manner. The miRNAs exhibiting the strongest response to low oxygen stress inhibit apoptosis and regulate neuroinflammation, likely providing neuroprotection. A principal component analysis (PCA) using a subset of the molecular targets assessed herein revealed differences between control and hypoxic groups for two solitary species (*Georychus capensis* and *Bathyergus suillus*), which are ecologically adapted to a normoxic environment, suggesting a heightened sensitivity to hypoxia relative to species that may experience hypoxia more regularly in nature. By contrast, all molecular data were included in the PCA to detect a difference between control and hypoxic populations of eusocial *Heterocephalus glaber*, indicating they may require many lower-fold changes in signaling pathways to adapt to low oxygen settings. Finally, none of the *Cryptomys hottentotus* subspecies showed a statistical difference between control and hypoxic groups, presumably due to hypoxia tolerance derived from environmental pressures associated with a subterranean and social lifestyle.

KEY WORDS: Hypoxia tolerance, Protein oxidation, DNA damage, HIF-1α, miRNA, Bathyergidae

INTRODUCTION

Metabolism in the adult brain is almost completely aerobic and the brain receives a large percentage of bodily oxygen from the blood supply (~12%), so changes in oxygen availability can have a substantial effect on brain function (Buck and Pamenter, 2018; Nortje and Gupta, 2006; Rolett et al., 2000). The critical oxygen tension is the partial pressure of oxygen (P_{O_2}) where O_2 consumption matches its delivery to the tissue, and it varies for each species, but it can also vary with angiogenesis, stress, exercise and hypoxia (Dunn et al., 2000). Hypoxia occurs when tissues do not receive an adequate oxygen supply and is a stress associated with some diseases such as cancer, stroke and cardiac arrest (Buck and Pamenter, 2018). Below the critical oxygen tension, a decrease in ATP is accompanied by a rise in ADP and AMP (Ashcroft and Ashcroft, 1990; Folbergrová et al., 1990). Hypoxia/ischemia cause reductions in ATP levels within a few minutes which can have an impact on cellular health (Ashcroft and Ashcroft, 1990; Buck and Pamenter, 2018). Hypoxia also creates a favorable environment for the generation of free radicals and their leakage from the mitochondria into the cytosol and extracellular space, which has the potential of causing significant cell damage to membranes, proteins, lipids and other cellular components (Smith et al., 2017; Terraneo et al., 2017). Free radicals are also produced upon reoxygenation. However, several mole-rat species such as *Spalax galili* and *Heterocephalus glaber* are resistant to decreases in oxygen tension (Larson and Park, 2009; Schülke et al., 2012; Shams et al., 2004), and other species of African mole-rats (Bathyergidae) may also show hypoxia tolerance (Ivy et al., 2020).

African mole-rats spend the majority of their life in subterranean environments where oxygen concentration may be as low as 15% (McNab, 1966). They have developed mechanisms to adapt to their hypoxic, hypercapnic and high ammonia tunnel systems where they are able to tolerate extremely low oxygen tensions for several hours without any significant cellular damage (Johansen et al., 1976; Larson and Park, 2009). Some species of African mole-rats, like the naked mole-rat (*H. glaber*), have been shown to tolerate P_{O_2} of 3% or lower, for several hours (Pamenter et al., 2018; Park et al., 2017), and respond with a decrease in oxygen consumption of 85% and a reduction in neuronal electron transport chain by 50% relative to normoxic controls (Pamenter et al., 2015, 2018).

This study focused on the hypoxia tolerance of six species of African mole-rats: the Cape dune mole-rat [*Bathyergus suillus* (Schreber 1782)], three subspecies of the common mole-rat [*Cryptomys hottentotus hottentotus* (Lesson 1826), *Cryptomys hottentotus mahali* (Roberts 1913) and *Cryptomys hottentotus pretoriae* (Roberts 1913)], the Cape mole-rat [*Georychus capensis* (Pallas 1778)] and the naked mole-rat (*H. glaber* Rüppell 1842). Phylogenetic analyses have concluded that *H. glaber* is the ancestral species of the Bathyergidae family, whereas mole-rats of the genus *Cryptomys* evolved more recently (~6–7 mya) (Fig. 1) (Faulkes et al., 2004). Naked mole-rats were the first mammalian species identified as being eusocial (having a social structure with a queen and workers) (Jarvis, 1981). They burrow in very dry, hard soil, and

[1]Institute of Biochemistry and Department of Biology, Carleton University, Ottawa, ON, Canada, K1S 5B6. [2]Mammal Research Institute and Department of Zoology & Entomology, University of Pretoria, Hatfield, Pretoria 0028, South Africa. [3]Department of Biology, University of Ottawa, Ottawa, ON, Canada, K1N 6N5. [4]Ottawa Brain and Mind Research Institute, University of Ottawa, Ottawa, ON, Canada, K1H 8M5.
*These authors contributed equally to this work

‡Author for correspondence (kenstorey@cunet.carleton.ca)

S.M.L., 0000-0002-3065-3155; K.E.S., 0000-0001-8002-1853; N.C.B., 0000-0001-9748-2947; D.W.H., 0000-0002-4592-558X; B.v., 0000-0001-5154-5922; M.E.P., 0000-0003-4035-9555; K.B.S., 0000-0002-7363-1853

Received 29 October 2019; Accepted 30 January 2020

Journal of Experimental Biology (2020) 223, jeb215905. doi:10.1242/jeb.215905

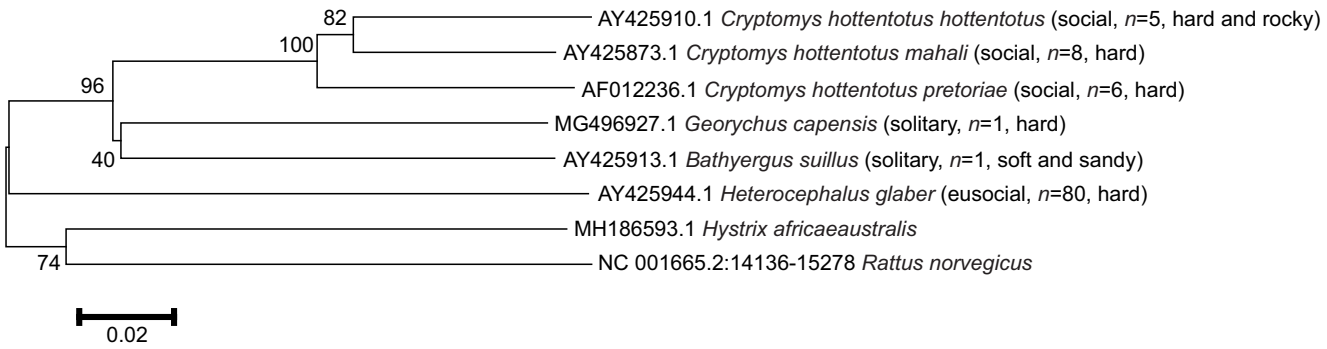

Fig. 1. Phylogenetic tree of cytochrome *b* sequences from the six species of African mole-rat compared with those of a lab rat and an African porcupine. Accession numbers are given before the species name. Sociability, the average size of the colony (*n*) and the hardness of the soil are indicated following the species name in parentheses. The bootstrap values at the nodes were obtained from 10,000 bootstrap replicates and are reported as percentages. The scale bar corresponds to 0.02 change per nucleotide.

because of their characteristic lack of fur, are poor endotherms. Living in large eusocial colonies would help the naked mole-rat thermoregulate, but it would also contribute to increased O_2 consumption and higher CO_2 production in closed-off burrows, which theoretically could trigger a higher hypoxia tolerance in the naked mole-rat (Tregub et al., 2013). By contrast, the closely related *B. suillus* and *G. capensis* species are strictly solitary and must dig their less-complex tunnel systems alone. The hypoxia tolerance of these solitary species may differ as a result of differences in the soils they reside in; *B. suillus* live in soft, sandy soils, which are porous to air and water, but are easier for this large species to dig in; *G. capensis* occur in harder soils that are less porous to air and water and would require more effort to move through, and therefore heightened respiration (Thomas et al., 2009, 2013). In addition, these two species are known to occasionally emerge from their tunnel systems and forage on the surface; this is most frequently seen in *B. suillus*. *Cryptomys*, in contrast, is a social genus of mole-rat that has a large range, partially because it is one of the most specious genera (Ingram et al., 2004). Although *C. h. hottentotus* and *G. capensis* have different levels of sociability, they have similar lifestyles and spend most of their time in their nests, estimated as 81% and 90% of their time, respectively (Bennett, 1992). However, *Cryptomys* species live in much harsher environments and burrow in packed, rocky ground. *Cryptomys hottentotus* species would therefore be expected to be the most hypoxia-tolerant species, as a result of living in social colonies, rarely coming to the surface, and digging in harder soils than *G. capensis*: factors that would result in increased levels of CO_2 in their sealed-off tunnel systems.

In order to assess the mole-rats' ability to tolerate hypoxic stress at the molecular level, several molecular markers of cell stress and microRNA (miRNA) profiles were measured in the brains of these six species, comparing normoxic and hypoxic conditions. Specifically, miRNAs that are upregulated in response to hypoxia were investigated in the six species of African mole-rat, with most having roles in regulating cell death, inflammation and angiogenesis (Kulshreshtha et al., 2007; Truettner et al., 2013). Hypoxia damage to the brain was estimated by analyzing relative protein carbonylation and 8-hydroxy-2′-deoxyguanosine (8-OH-dG) levels. Protein carbonylation, an irreversible modification that most often occurs on cysteine and methionine residues, is a biomarker of oxidative stress that occurs in disease (Alzheimer's, ischemia–reperfusion) and natural aging (Dalle-Donne et al., 2006). 8-OH-dG has been established as a strong indicator of hypoxia-induced tissue damage and can be detected in both the brain tissue and urine of mammals exposed to acute hypoxia and ischemic stroke (Nair et al., 2012; Nakajima, 2012). Based on reports of altered antioxidant enzyme levels and activity in selected normoxic mole-rat species relative to other rodent species (Andziak et al., 2006; Caballero et al., 2006; Fang et al., 2014; Schmidt et al., 2016), overall antioxidant capacity was also assessed to determine whether mole-rat species increase the use of antioxidants to prevent damage in response to oxidative stress. Protein levels of the hypoxia-inducible transcription factor (HIF-1α) and its binding capacity to DNA were also evaluated to determine whether hypoxia signaling differed among the six species. Finally, the relative expression of 27 miRNAs that have been linked with low oxygen adaptation in other mammals was assessed. The results suggested that the mole-rat species examined respond to hypoxia in a species-specific manner, where the species with the lowest tolerance to low oxygen would also be the least likely to experience hypoxia in the wild.

Overall, this study investigated whether different mole-rat species experience damage induced by hypoxia (oxidized protein and DNA markers), and explored the mechanisms they may use to tolerate hypoxia (HIF-1α DNA binding and protein levels, miRNA, antioxidant capacity), which may provide insight into the treatment and prevention of human diseases involving hypoxic insults, such as stroke and cardiac arrest. Furthermore, understanding how naturally occurring hypoxia-tolerant animals deal with hypoxia at the molecular level will help in the development of treatments for solid cancer tumors, as hypoxia is a common characteristic of locally advanced solid tumors that has been associated with diminished therapeutic response and malignant progression.

MATERIALS AND METHODS

Animal protocols

Except for naked mole-rats, which came from a laboratory-raised colony, all other mole-rat species were wild-captured in South Africa with permits and the experimental procedures that were approved by the animal ethics committee of the University of Pretoria (EC069-17). Mean body mass of the animals was: *C. h. mahali* 109.1±6.6 g, *C. h. pretoriae* 114.8±12.3 g, *C. h. hottentotus* 78.7±5.5 g, *B. suillus* 587.0±90.8 g, *G. capensis* 133.2±19.0 g and *H. glaber* 51.3±3.7 g. Wild-caught mole-rats (randomly separated into *n*=4 groups of control and hypoxic animals) were acclimated to laboratory conditions 3 weeks prior to the hypoxic exposures, using a simulated 12 h light:12 h dark cycle and with food supplied *ad libitum*. For hypoxia exposures, animals were placed individually and unrestrained inside 4.7 l (*B. suillus*) or 1 l (all other species) Plexiglas chambers held at ∼28°C. Animals were provided with

Journal of Experimental Biology (2020) 223, jeb215905. doi:10.1242/jeb.215905

a thin layer of bedding on the floor of the experimental chamber. The chamber was sealed and constantly supplied with dried incurrent air and nitrogen, mixed to the desired fractional gas composition by pre-calibrated rotameters (Matheson Model 7400 Gas Mixer, E700 and E500 flowtubes, Oakville, ON, Canada) at a flow rate of 600 ml min^{-1} (small chamber) or 2 l min^{-1} (large chamber), which was assessed by a calibrated mass flow meter (Alicat Scientific, Tucson, AZ, USA). Excurrent air flow leaving the animal chamber was continuously subsampled at 200 ml min^{-1}, with water vapor measured with a water vapor analyzer (RH-300, Sable Systems, Las Vegas, NV, USA), dried with pre-baked drierite (Drierite, W.A. Hammond Drierite Co. Ltd, Xenia, OH, USA), and analyzed for O_2 and CO_2 fraction using a galvanic fuel cell O_2 analyzer and infrared CO_2 analyzer (FOXBOX, Sable Systems).

Naked mole-rats were group-housed in interconnected multi-cage systems at 30°C and 21% O_2 in 70% humidity with a 12 h light:12 h dark cycle. Animals were fed fresh tubers, vegetables, fruit and Pronutro cereal supplement *ad libitum*. Animals were not fasted prior to experimental trials. All experimental procedures were approved by the University of Ottawa Animal Care Committee in accordance with the Animals for Research Act and by the Canadian Council on Animal Care. Non-breeding (subordinate) naked mole-rats do not undergo sexual development or the expression of sexual hormones and thus we did not take sex into consideration when evaluating our results (Holmes et al., 2009).

Animals were randomly assigned to either (i) 3 h of normoxia (21 kPa O_2, balance N_2; control) or (ii) 3 h of hypoxia at 5 kPa O_2 for most species or 7 kPa O_2 for *B. suillus*; exposures were preceded by a 30 min step at 12 kPa O_2. Hypoxia exposures were chosen to be just above the low oxygen minimum that the animals withstood in preliminary experiments (Ivy et al., 2019). Following experimentation, animals were euthanized immediately by cervical dislocation followed by decapitation and brain samples were extracted on ice and stored at −80°C until analyzed.

Total protein extraction

Whole frozen brain from n=4 control and n=4 hypoxic animals of each species was weighed (~60–80 mg) and crushed into small pieces under liquid nitrogen. Tissue samples were homogenized 1:4 w:v in Cell Signaling lysis buffer (Millipore-Sigma, 43-040) supplemented with 1 mmol l^{-1} sodium orthovanadate, 10 mmol l^{-1} sodium fluoride, 10 mmol l^{-1} β-glycerophosphate and 10 µl ml^{-1} Protease Inhibitor cocktail (BioShop, PIC001.1) using a Polytron PT10 homogenizer. Each sample was placed on ice, sonicated for 10 s, and then gently vortexed every 10 min for 30 min before centrifugation at 13,500 ***g*** for 20 min at 4°C. The supernatant containing soluble proteins was collected and total protein concentration was determined for ELISA samples using the Bio-Rad method (Bio-Rad, 500-0005). Samples for the protein carbonylation assay were standardized to 3 µg $µl^{-1}$, samples for the HIF-1α transcription factor DNA binding activity assay were standardized to 1 µg $µl^{-1}$, and samples for the total HIF-1α assay were standardized to 20 µg $µl^{-1}$ for all species except for *H. glaber*, which were standardized to 16.5 µg $µl^{-1}$ by adding appropriate amounts of Cell Signaling lysis buffer. Protein samples for the antioxidant capacity assay were diluted to 2.2 µg $µl^{-1}$ in antioxidant assay buffer provided with the kit.

Protein carbonylation assay

Protein carbonylation (Cayman Chemical Company, 10005020) was assessed as per the kit manufacturer's instructions. The amount of protein-hydrazone produced from the reaction of 2,4-dinitrophenylhydrazine (DNPH) with protein carbonyls in tissue homogenates was quantified spectrophotometrically as a measure of protein carbonyl content. For each sample from normoxic and hypoxic individuals, 100 µl of total protein extract was standardized to 3 µg $µl^{-1}$ and then treated with either 400 µl of DNPH (experimental) or 400 µl 2.5 mol l^{-1} HCl (control). Both experimental and control solutions were incubated in the dark at room temperature (RT) for 1 h with intermittent vortexing every 15 min. Then, 0.5 ml of 20% TCA solution was added to each sample and vortexed, followed by a 5 min incubation on ice and then centrifugation at 10,000 ***g*** for 10 min at 4°C. The supernatant was discarded and the pellet resuspended in 0.5 ml of 10% TCA and placed on ice. Samples were centrifuged again, and the pellet was resuspended in 0.5 ml 1:1 v:v ethanol/ethyl acetate followed by vortexing and centrifugation at 10,000 ***g*** for 10 min at 4°C. This step was repeated two more times. Next, protein pellets were resuspended in 250 µl guanidine hydrochloride, centrifuged again under the same conditions and 220 µl of the supernatant from each sample was transferred to a separate well of a 96-well microplate. Absorbance was measured at 370 nm and the signal from each control well was subtracted from the signal of the corresponding experimental well. Protein carbonyl concentration (nmol ml^{-1}) was then calculated as per the manufacturer's instructions.

Antioxidant capacity assay

Antioxidant capacity was assayed using a commercially available kit (Cayman Chemical Company, 709001), which utilizes the ability of antioxidants in the sample to inhibit the oxidation of ABTS [2,2′-azino-di-(3-ethylbenzthiazoline sulfonate)] to $ABTS^{+}$. A standard curve was prepared by combining increasing amounts of Trolox (6-hydroxy-2,5,7,8-tetramethylchoman-2-carboxylic acid) diluted in antioxidant assay buffer (5 mmol l^{-1} potassium phosphate, pH 7.4, with 0.9% sodium chloride and 0.1% glucose) to obtain concentrations between 0 and 0.330 mmol l^{-1}. Briefly, 10 µl of Trolox solution or 2.2 µg $µl^{-1}$ protein samples was combined with 10 µl of metmyoglobin and 150 µl of chromogen. Reactions were initiated by addition of 40 µl of the hydrogen peroxide working solution and were incubated on a shaker in the dark for 5 min at RT. Absorbance was read at 750 nm and quantified as Trolox equivalents (mmol l^{-1} mg^{-1} wet mass).

HIF transcription factor ELISA

An assay for HIF-1α transcription factor DNA binding activity was performed as directed by the manufacturer (Abcam, ab133104), using total protein extracts prepared as above. To ensure the signal detected was indeed due to HIF-1α binding to DNA, one well containing $NiCl_2$-stimulated HeLa cell nuclear extract was used as a positive control and another contained competitive dsDNA. The blank contained the 1× antibody binding buffer (ABB) but no antibodies, and non-specific binding was assessed via the use of wells that contained the 1× ABB and both primary and secondary antibodies. To each well, 10 µl of each control or hypoxia protein extract was added along with 90 µl of complete transcription factor binding assay buffer. The plate was sealed and incubated overnight at 4°C. The wells were washed as directed before adding 100 µl of transcription factor (TF) HIF-1α primary antibody (1 in 100 using 1× ABB) to each well, except the blank wells. The plate was sealed and incubated for 1 h at RT, then washed and 100 µl of TF goat anti-rabbit HRP conjugate secondary antibody (1 in 100 using 1× ABB) was added to all wells except the blank, followed by incubation for 1 h at RT. The plate was washed as directed and then

100 µl of TF developing solution was added to each well followed by incubation for 45 min at RT with gentle agitation while protected from light. Once wells were visibly blue, 100 µl of TF stop solution was added and absorbance readings were obtained at 450 nm using a plate reader.

HIF total protein ELISA

HIF-1α protein abundance was determined with a commercially available HIF-1α ELISA kit (Abcam, ab171577). All buffers, reagents and standards were prepared according to the manufacturer's instructions. First, a HIF protein standard with a stock concentration of 200 ng ml^{-1} was diluted in cell extraction buffer to concentrations between 15 and 0.23 ng ml^{-1}. Protein lysates standardized to 20 µg µl^{-1} (or 16.5 µg µl^{-1} for *H. glaber* samples) and standards were added to their appropriate wells, with an equal volume of 1× antibody cocktail (a mixture of capture and detection antibodies). The plate was sealed and incubated for 1 h at RT on a plate shaker. Next, each well was rinsed 3 times with 350 µl of 1× prepared wash buffer ensuring complete removal of liquid after each wash. Then, 100 µl of TMB substrate was added to each well and incubated for 10 min in the dark on a plate shaker, followed by addition of 100 µl of stop solution to each well and shaking for 1 min to mix. Optical density (OD) was then measured at 450 nm using a plate reader.

DNA extraction and 8-OH-dG assay

DNA was extracted from both normoxic and hypoxic mole-rats (n=4 each) using a Quick-DNA Plus Kit (Zymo Research, D4068) according to the manufacturer's instructions. Briefly, samples weighing 25 mg were lightly homogenized in proteinase K solution (47.5% solid tissue buffer, 5% proteinase K) using a glass pestle and then digested overnight. The next day, 400 µl of genomic binding buffer was added to each sample, followed by 10–15 s vortexing. Samples were then transferred to a Zymo-Spin™ column and centrifuged at 12,000 ***g*** for 1 min. The flow through was discarded, and 400 µl of DNA pre-wash buffer was added. After another centrifugation, a total of 900 µl of g-DNA wash buffer was used to wash the collected DNA. Finally, the DNA was eluted from the column after a 5 min incubation in 50 µl of DNA elution buffer. The DNA was digested by incubation at 55°C for 1 h with 4 U of nuclease P1 (Millipore-Sigma, N8630). To digest nucleotides to nucleosides, 1 U of alkaline phosphatase (NEB, M0290S) was added and each sample was incubated at 37°C for 30 min, then boiled for 10 min and placed on ice until use.

DNA/RNA oxidative damage ELISA was performed according to the kit manufacturer's instructions (Cayman Chemical, 589320). Standards were prepared from stock reagents supplied in the kit and reconstituted to concentrations from 10.3 to 3000 pg ml^{-1}. DNA samples from normoxic and hypoxic mole-rat brains were diluted in 1× ELISA buffer (Cayman Chemical, 400060) to 15 ng µl^{-1}. A non-specific binding blank (100 µl ELISA buffer, 50 µl tracer dye), a maximum binding blank (50 µl ELISA buffer, 50 µl tracer and 50 µl of monoclonal antibody) and a background absorbance blank (Ellman's reagent) were used. For both conditions and all six mole-rat species, 50 µl each of DNA, AChE tracer and monoclonal antibody specific to 8-OH-dG were combined into each well of the supplied microplate, covered with an adhesive strip and incubated overnight in the dark on a shaker at 4°C. Subsequently, the wells were washed 5× with wash buffer, 200 µl of Ellman's reagent was added and the plate was incubated for 90 min on a shaker at RT in the dark. OD was measured spectrophotometrically at 412 nm with blank subtraction.

Total RNA isolation

RNA isolation and miRNA amplification were performed as described previously (Biggar et al., 2018). Total RNA from mole-rat brains was isolated using Trizol™ (Invitrogen, 15596018). Briefly, 50 mg samples of tissue were each homogenized in 1 ml Trizol using a Polytron PT10 homogenizer. Next, 200 µl of chloroform was added followed by a 10 min incubation on ice and brief vortexing at low speed. Samples were then centrifuged at 10,000 ***g*** for 15 min at 4°C after which the upper aqueous layer was collected. RNA was precipitated with 500 µl of 2-propanol, followed by a 10 min incubation at RT, and centrifugation as above. The supernatant was removed and the pellet was washed with ethanol and centrifuged again. Excess ethanol was allowed to evaporate for 10 min. RNA pellets were then resuspended in 40 µl of sterile RNAse-free water. RNA purity was assessed by measuring the A_{260}/A_{280} ratio. RNA integrity was determined by visualizing 18S and 26S ribosomal bands on a 1% agarose gel with SybrGreen staining. All samples were diluted to 1.5 µg µl^{-1} using RNAse-free water.

cDNA synthesis and miRNA amplification

Polyadenylation was performed using a polymerase A tailing kit (Epi-Bio, PAP5104H). Reaction mixes were prepared with 1 µl of 10 mmol l^{-1} ATP, 0.5 µl *E. coli* polyadenylate polymerase (2 U) and 2 µg of total RNA, diluted with RNase-free water to a final volume of 10 µl. Reactions were incubated at 37°C for 30 min, then 95°C for 5 min, and transferred to ice. To ligate the stem-loop adapters to the RNA, 10 µl aliquots of polyadenylated RNA were incubated with 5 µl of 250 nmol l^{-1} universal stem-loop RT primer at 95°C for 5 min and then at 60°C for 5 min. After cooling on ice, reverse transcription was performed by adding 4 µl 5× first strand buffer (ThermoFisher Scientific, 18080044), 2 µl 0.1 mol l^{-1} DTT, 1 µl 25 mmol l^{-1} dNTP (ThermoFisher Scientific, R1121) and 1 µl M-MLV reverse transcriptase (2 U; ThermoFisher Scientific, 18080044) to each RNA sample. Reactions proceeded at 16°C for 30 min, 42°C for 30 min, followed by 85°C for 5 min. Finally, cDNA products were serially diluted and stored at −20°C until further use. The miRNAs to be evaluated were selected from the literature by doing searches on NCBI PubMed using keywords including miRNA, hypoxia and brain to identify numerous miRNAs that have been shown to be differentially expressed under hypoxia stress in rat brain (Truettner et al., 2013). The miRNAs of interest were evaluated for sequence conservation where the available mature miRNA stemloop sequences from *Mus musculus* obtained from miRBase database (release 22) were aligned with those of *H. glaber* using EMBL-EBI Clustal Omega. The universal reverse primer (5′-CTCACAGTACGTTGGTATCC-TTGTG-3′) and the forward primers listed in Table S1 were synthesized by Integrated DNA Technologies and were used in all qPCR reactions performed on a CFX96 real-time PCR detection system (BioRad Laboratories Inc.). Denaturation for 3 min at 95°C preceded 40 cycles of 95°C for 10 s and 60°C for 30 s. Melt curve analysis was used to confirm the amplification of a single amplicon.

Statistical analysis

For all analyses, data were analyzed by Student's t-test (n=4 independent replicates, P<0.05) to determine statistical significance between conditions (normoxia and hypoxia) for each species, independently of one another. All statistical analyses and figures were generated using RStudio or R-BioPlot (Zhang and Storey, 2016).

For each ELISA, the means (±s.e.m.) of the normoxic controls and hypoxic datasets for each species were calculated, and control

Journal of Experimental Biology (2020) 223, jeb215905. doi:10.1242/jeb.215905

values were normalized to 1 and the hypoxia mean was expressed relative to the normoxic control mean. In addition, a one-way ANOVA with a Tukey *post hoc* test (n=4 independent replicates, P<0.05) was used to compare the parameters assessed via ELISA between species at normoxic conditions. The analysis of HIF-1α protein levels excluded *H. glaber* because less total protein was used in the assay.

For all miRNAs examined, following amplification, expression data for the miRNAs of interest and the loading control were linearized using 2^{-Cq} as per the comparative ΔΔCq method. Sno-66 was used as the reference gene for all six species because its expression did not significantly change with hypoxia stress in any of the species (Student's *t*-test P>0.05). ΔΔCq was obtained by standardizing the miRNA expression data to the loading control. Then, the means of both normoxic and hypoxic miRNA data were generated. For each species, the normoxic (control) mean was normalized to 1 for graphing purposes and the hypoxia mean was expressed relative to the normoxic mean.

Principal component analysis (PCA) was computed in R using 'FactominR' version 1.41. Missing values were imputed using 'missMDA' version 1.14 (Josse and Husson, 2016). Relative protein, damage marker and gene expression data were used in the comparison of control and stress groups. Then, the top five contributing factors for each principal component were identified by the function fviz_contrib using choice='var'. These are reported in Table S3.

RESULTS

Markers of protein and DNA damage

The relative protein carbonylation level did not change in any of the six mole-rat species in response to hypoxia exposure (Fig. 2). Furthermore, there were no changes in the level of 8-OH-dG after hypoxia in any of the species (Fig. 3).

Antioxidant capacity

There was no significant change in antioxidant capacity comparing normoxia controls and hypoxia conditions for any of the species (Fig. 4A). However, when comparing all species in normoxia, antioxidant capacity was the only parameter assessed via ELISA to show statistical significance between species, with *C. h. mahali* having 2.11(±0.28)-fold increased antioxidant capacity relative to *B. suillus*.

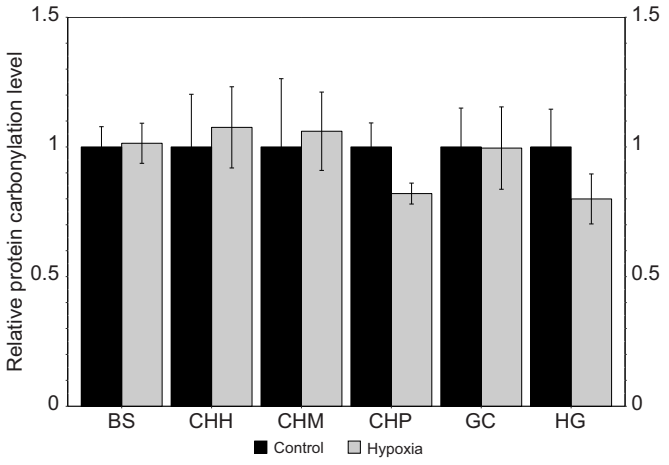

Fig. 2. Relative protein carbonylation level in the brain of normoxic (control) and hypoxic mole-rats. BS, *Bathyergus suillus*; CHH, *Cryptomys hottentotus hottentotus*; CHM, *Cryptomys hottentotus mahali*; CHP, *Cryptomys hottentotus pretoriae*; GC, *Georychus capensis*; and HG, *Heterocephalus glaber*. Data are means±s.e.m., with the normoxic mean normalized to 1; n=4 biological replicates from brains of different animals.

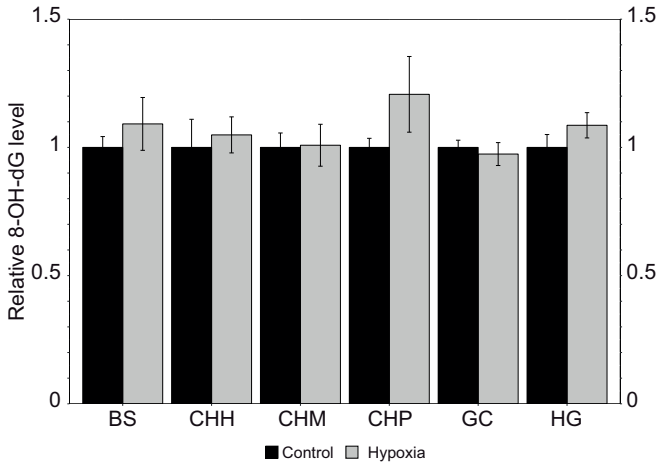

Fig. 3. Relative 8-hydroxy-2′-deoxyguanosine (8-OH-dG) levels in double-stranded DNA from normoxic control and hypoxic brain of the six mole-rat species. Other information as per Fig. 2.

Hypoxia-inducible factor

The protein levels and transcription factor DNA-binding activity of HIF-1α were examined (Figs 5 and 6, respectively) and revealed species-specific results. Total HIF-1α levels increased in response to hypoxia exposure in both *B. suillus* and *C. h. hottentotus* to 3.26(±0.25)-fold and 2.59(±0.18)-fold, respectively, over normoxic controls, but were unchanged in the other species (Fig. 5). However,

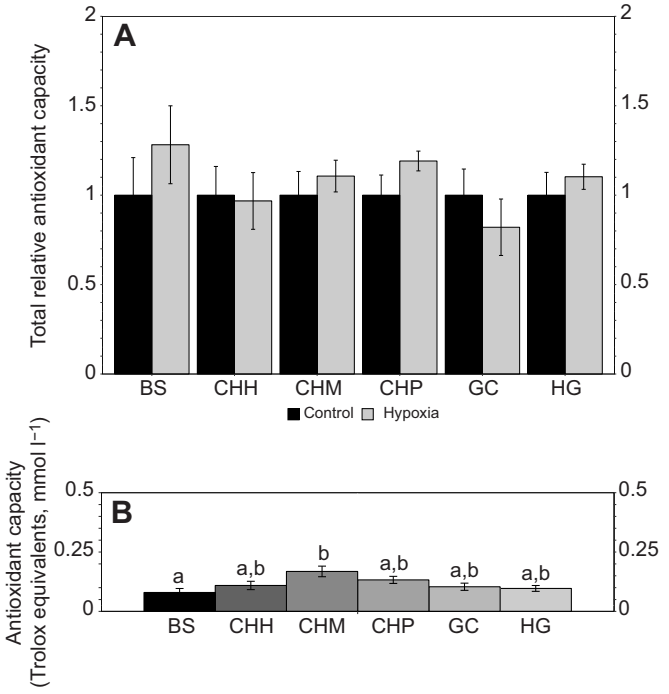

Fig. 4. Total antioxidant capacity in the six species of mole-rat. (A) Histogram comparing relative antioxidant capacity of control and hypoxic mole-rats (other information as per Fig. 2). (B) Histogram comparing baseline (normoxic) levels of antioxidant capacity (Trolox equivalents) across species using a one-way ANOVA with a Tukey *post hoc* test (P<0.05). Different letters indicate statistical significance.

Journal of Experimental Biology (2020) 223, jeb215905. doi:10.1242/jeb.215905

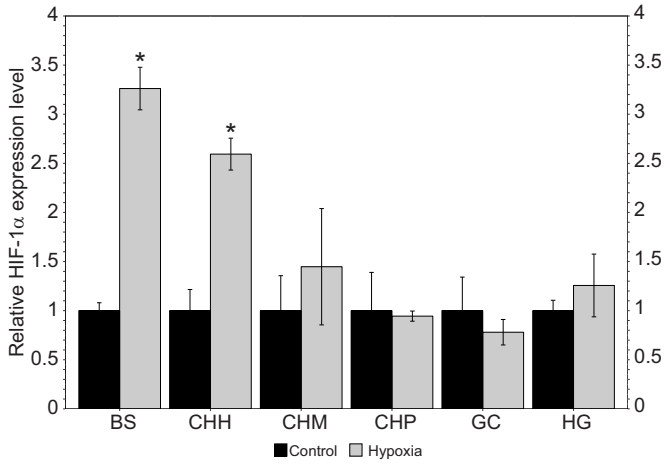

Fig. 5. Relative HIF-1α protein abundance in brain tissue of normoxic control and hypoxic mole-rats. Other information as per Fig. 2. Asterisks indicate data that are significantly different from the control condition (P<0.05).

HIF-1α transcription factor binding activity did not change in any of the mole-rat species in response to hypoxia (Fig. 6).

miRNA

The levels of 27 miRNAs that have been implicated in hypoxia-related processes were evaluated in the brain of all six mole-rat species. Fig. 7 is a heat map comparing the species whereas Fig. S1 shows the individual data for each species and Table S3 summarizes the roles of miRNAs chosen for this study. The greatest number of significant changes in miRNAs occurred in *B. suillus*, with strong upregulation of 19 miRs ranging from 1.72(±0.18)-fold to 14.6(±4.04)-fold, as compared with controls. In *C. h. hottentotus*, only two significant changes were noted, a 2.07(±0.27)-fold increase in miR-125b-5p and a decrease in miR-24-3p levels to 69±7.1% of control values (Fig. 7; Fig. S1B). The brain of *C. h. mahali* showed decreased expression of three miRNAs: miR-210-3p, miR-150-5p and miR-592-3p decreased to 53±13%, 48±14% and 58±12% of control values, respectively (Fig. 7; Fig. S1C). However, the brain of the related *C. h. pretoriae* did not differentially express any miRNAs in response to hypoxia (Fig. 7; Fig. S1D).

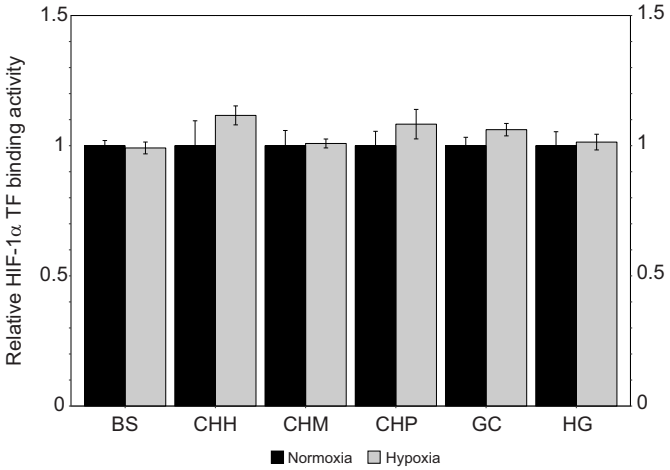

Fig. 6. Relative HIF-1α transcription factor (TF) binding activity in brain tissue from normoxic control and hypoxic mole-rats. Other information as per Fig. 2.

The Cape mole-rat, *G. capensis*, significantly changed the levels of 9 of the 27 miRNAs assessed. Levels of four miRNAs increased (miR-147-3p, miR-150-5p, miR-199a-3p and miR-325-5p) with changes ranging from 1.54- to 3.31-fold compared with the control value. Five miRNAs decreased in expression (miR-24-5p, miR-24-3p, miR-27a-3p, miR-140-5p and miR-146a-3p), with levels reduced to 22–43% of the normoxic mean (Fig. 7; Fig. S1E). Finally, the brain of *H. glaber* significantly increased five miRNAs in response to hypoxia with values ranging from 1.27- to 2.17-fold the normoxic value for miR-24-5p, miR-24-3p, miR-207, miR-27a/b-3p and miR-592-3p (Fig. 7; Fig. S1F). In contrast, three miRNAs (miR-210-5p, miR-26b-5p and miR-126a-5p) were suppressed by 31–52%.

PCA plots

PCA plots were used to uncover the underlying trends in the molecular data. There were no statistical differences between control and hypoxic groups of any of the three *Cryptomys hottentotus* subspecies when considering all molecular data (Fig. S2) or when only mapping the trends from the top five contributing factors for PC1 and PC2 (Table S2; Fig. 8). The molecular markers that we used were sufficient to identify major differences between control and hypoxic mole-rats for the three other species, *B. suillus*, *G. capensis* and *H. glaber*. However, when considering only the top five contributing variables for these three species, the significant difference between control and hypoxia was only seen for *B. suillus* and *G. capensis*.

When comparing the molecular data of hypoxic animals from all species, it was observed that *B. suillus* was different from all other species (Fig. 9); the top five variables for each principal component are shown for clarity.

DISCUSSION

In this study, we evaluated the relative expression of molecular markers linked to hypoxia in the brains of six species of mole-rats to determine how various African mole-rat species respond to hypoxia. Firstly, it was interesting that none of the mole-rat species showed increased oxidative damage during hypoxia (Figs 2 and 3). The unchanging level of protein carbonylation and 8-OH-dG DNA during hypoxia suggests that mole-rats may use mechanisms to limit oxidative damage and/or remove the by-products of reactive oxygen species (ROS) reactions. Analysis of liver and urinary metabolites suggests that mole-rats accumulate more oxidized protein, lipid and DNA than hypoxia-intolerant mice, possible as a result of having 70-fold lower liver glutathione peroxidase (GPx) activity levels than mice in normoxic conditions (Andziak et al., 2005). Even though mice have highly active GPx and high antioxidant enzyme gene expression at normal oxygen levels, mice exposed to 9% oxygen still showed increased protein carbonylation and other markers of oxidative injury (Veasey et al., 2004). Recently, research has shown *H. glaber* muscle and heart can detoxify mitochondrial ROS better than those of mice in normoxic conditions, suggesting enhanced tissue-specific antioxidant capabilities (Munro et al., 2019). Brain from anoxia-tolerant turtles and mole-rats increases or maintains high gene/protein expression and enzyme activity levels of antioxidant enzymes other than GPx in low oxygen conditions, which may help them handle episodic oxidative stress (Andziak et al., 2006; Schülke et al., 2012; Willmore and Storey, 1997). Herein, all six species also showed no change in global antioxidant capacity with hypoxia (Fig. 4). Sustained antioxidant capacity in conjunction with no change in oxidative damage of DNA or protein during hypoxia is

Journal of Experimental Biology (2020) 223, jeb215905. doi:10.1242/jeb.215905

	BS	CHH	CHM	CHP	GC	HG
hgl-let-7f-5p	**10.30**	1.38	0.87	1.57	1.12	0.61
hgl-miR-210-5p	2.22	0.94	0.78	1.23	1.69	**0.48**
hgl-miR-210-3p	**7.54**	0.95	**0.53**	1.34	1.75	1.20
hgl-miR-17-3p	2.15	0.95	1.08	0.81	1.49	1.31
hgl-miR-24-5p	3.20	0.72	0.89	1.05	**0.43**	**1.94**
hgl-miR-24-3p	**5.37**	**0.69**	0.89	1.18	**0.26**	**2.17**
hgl-miR-26b-5p	**14.65**	1.00	1.35	2.43	1.45	**0.53**
hgl-miR-27a-5p	**3.38**	0.77	0.79	1.21	1.58	0.80
hgl-miR-27a-3p	**6.44**	1.01	0.62	1.50	**0.33**	**2.15**
hgl-miR-124-3p	**13.73**	1.12	1.11	3.10	0.73	0.65
hgl-miR-125b-5p	**5.39**	**2.07**	1.09	2.31	1.94	0.73
hgl-miR-126a-5p	**5.63**	1.07	2.18	1.23	0.59	**0.69**
hgl-miR-140-5p	2.82	0.90	0.57	1.39	**0.28**	0.81
hgl-miR-140-3p	**2.12**	1.23	0.84	1.28	1.37	0.81
hgl-miR-146a-5p	**2.22**	0.87	0.60	1.06	0.66	1.29
hgl-miR-146a-3p	1.46	0.82	0.70	1.11	**0.39**	0.67
hgl-miR-147-3p	**1.73**	1.02	0.94	1.49	**3.31**	–
hgl-miR-150-5p	1.71	0.97	**0.48**	2.10	**2.16**	1.50
hgl-miR-199a-3p	**1.76**	0.98	0.69	0.92	**1.54**	1.84
hgl-miR-207	1.72	0.75	0.71	1.04	1.42	**1.66**
hgl-miR-325-3p	**2.08**	0.88	0.62	1.07	1.64	1.07
hgl-miR-325-5p	**2.23**	0.80	0.61	1.23	**1.63**	1.51
hgl-miR-376a-3p	0.69	1.01	1.08	1.13	1.81	1.03
hgl-miR-378-3p	**7.92**	1.37	0.81	2.40	1.57	0.96
hgl-miR-378-5p	**2.66**	1.18	0.80	1.09	0.84	0.81
hgl-miR-592-3p	**4.66**	1.03	**0.58**	1.05	1.56	**1.27**
hgl-miR-592-5p	**1.93**	0.78	1.29	0.98	1.15	0.85

Scale

0.00	0.25	0.75	1.00	2.00	4.00	6.00

Fig. 7. Heat map showing relative miRNA expression levels in brain of hypoxic mole-rats relative to normoxic controls. White tiles show values for hypoxia that did not differ from controls (set to 1 for graphing purposes) whereas blue tiles show decreases and red tiles increases in miRNA expression levels relative to controls. Bold values represent significant differences compared with normoxic controls. Scale represents the range of fold-changes. Species included in the miRNA analysis are listed as per Fig. 2.

consistent with these previous reports of constitutively high and increased expression and activity patterns of certain, but not all, antioxidant enzymes in animals treated with hypoxia. Further, the relatively short time frame of the hypoxia exposure (3 h) in the current study may not have necessitated an enhancement of antioxidant defenses. Increased antioxidant capacity may be more important upon reoxygenation, which was not studied herein. Interestingly, antioxidant capacity was the only parameter to significantly differ between different species in normoxic conditions. Specifically, *C. h. mahali* had over 2-fold higher antioxidant capacity than *B. suillus*, suggesting different mole-rat species may have different baseline antioxidant capacities to help them adapt to different levels of natural hypoxic exposures. Also, considering *B. suillus* had a reduced capacity to withstand experimental hypoxic exposures as severe as those tolerated by *C. h. mahali*, *B. suillus* may have a lower antioxidant capacity in normoxia because this solitary species does not encounter low oxygen environments as regularly as the more social *C. h. mahali* might, in the wild.

Instead of using increased antioxidant capacity, mole-rat tissues (including brain) may minimize accumulation of damaged proteins by removing them as they are formed, as evidenced by greater protein ubiquitination and proteasome activity compared with that in mice (Garbarino et al., 2015; Perez et al., 2009). Mole-rats may also use comparable mechanisms to minimize or prevent the accumulation of DNA damage. As previously mentioned, mole-rats may increase the activity of certain antioxidant enzymes to prevent DNA oxidation. Similar to the Spalacidae family of mole-rats, Bathyergidae mole-rats may have genomic differences compared with hypoxia-intolerant and terrestrial rodents that allow them to express DNA repair proteins under hypoxia stress (Shams et al., 2013). Compared with hypoxia-intolerant species, *H. glaber* have a higher copy number of the two genes (*TINF2* and *CEBPG*) that are involved in protecting DNA integrity and repairing damaged DNA, and they show more efficient nucleotide and base excision repair and PARylation activities than mouse cells in response to both H_2O_2 and UV irradiation damage to DNA (Evdokimov et al., 2018; Macrae et al., 2015). Overall, the lack of change in DNA and protein oxidation in response to hypoxia in the six species analyzed in the present study supports the concept that mole-rats have evolved unique molecular mechanisms that suit them for subterranean life under low oxygen conditions.

HIF-1α levels increased strongly in the brains of *B. suillus* and *C. h. hottentotus* under hypoxia, providing an indication that O_2 levels in the brains of these two species were at or below a crucial low O_2 tension that necessitated a metabolic response to alleviate hypoxia, which may indicate variability in hypoxia resistance among the six species. *Bathyergus suillus* and *C. h. hottentotus* happen to have overlapping ecological niches (Thomas et al., 2013) and *C. h. pretoriae* and *C. h. mahali* do not, even though they are more closely related. This suggests that the environment may influence the molecular mechanisms that are utilized for hypoxia tolerance. *Bathyergus suillus* and *C. h. hottentotus* may upregulate HIF-1 to enhance glycolysis by directly inducing transcription of the glucose transporter (GLUT1) and several glycolytic enzymes as well as upregulating pyruvate dehydrogenase kinase 1 (PDK1) to inhibit pyruvate catabolism by the tricarboxylic acid cycle, and thereby promote lactate production as the end product of glycolytic

Journal of Experimental Biology (2020) 223, jeb215905. doi:10.1242/jeb.215905

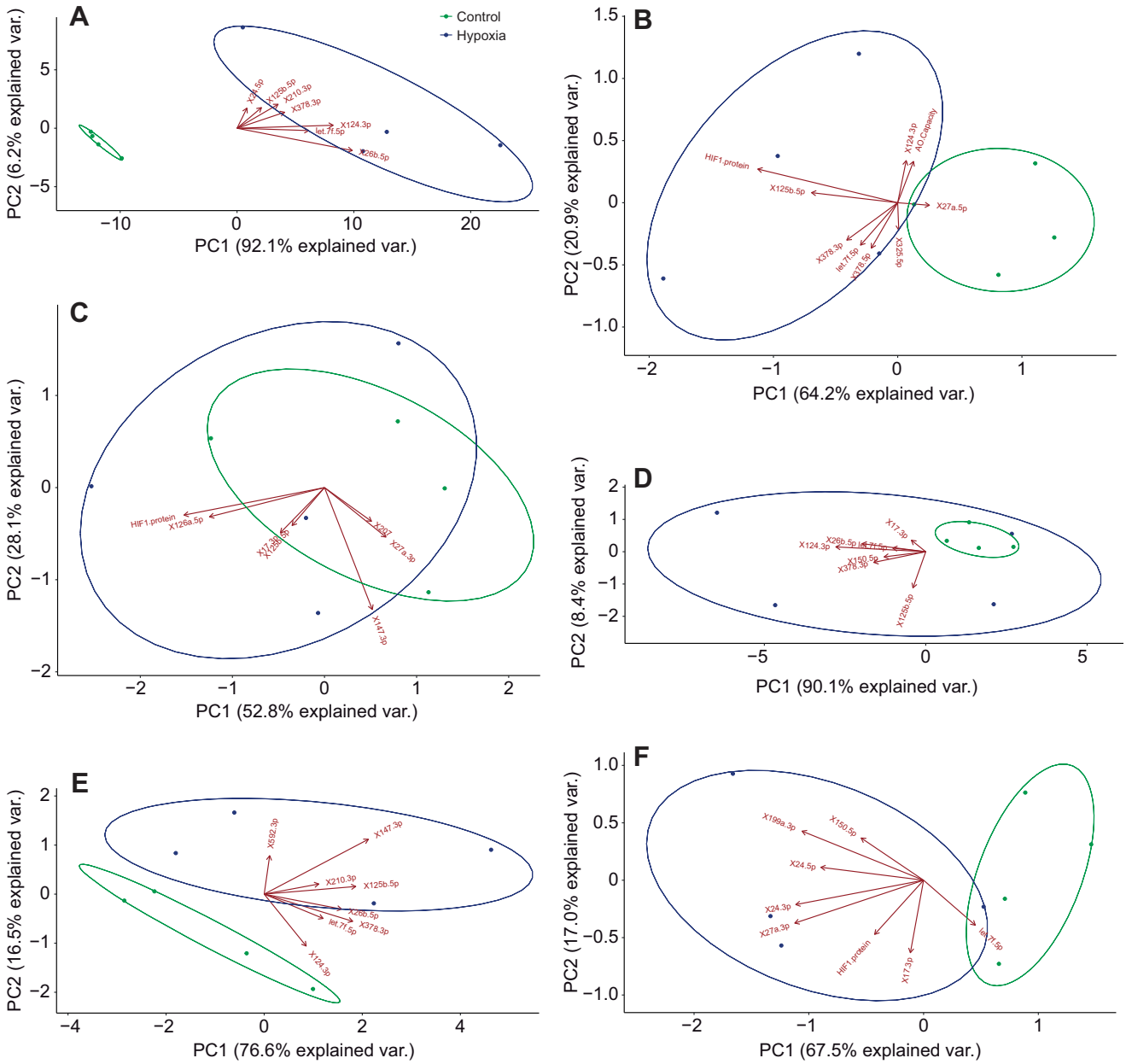

Fig. 8. Principal component analysis (PCA) of the molecular data from each individual mole-rat species. PCA plots correspond to each species (A, *B. suillus*; B, *C. h. hottentotus*; C, *C. h. mahali*; D, *C. h. pretoriae*; E, *G. capensis*; and F, *H. glaber*) and show how normalized data from control (green ellipse) and hypoxic (blue ellipse) groups cluster when considering only the top five contributing factors for PC1 and PC2. Additional factors were not considered if there was an overlap between the PC1 and PC2 contributing factors.

ATP production (Mirtschink and Krek, 2016; Papandreou et al., 2006). Under normoxic conditions, HIF-1α levels are very low as a result of rapid degradation by the ubiquitin-proteasome system whereas HIF-1β is constitutively expressed. During hypoxia, however, HIF-1α levels are stabilized, leading to the formation of the HIF-1 dimer and then HIF-1 binding to the hypoxia response element (HRE) of target genes to upregulate their transcription (Dengler et al., 2014). HIF-1α from *H. glaber* may have amino acid substitutions that prevent HIF-1α ubiquitination and degradation such that it may be constitutively expressed (Kim et al., 2011; Xiao et al., 2017), which could help explain why HIF-1α protein levels were simply maintained in the other four African mole-rat species. Xiao et al. (2017) also demonstrated that HIF-1α protein levels only increased following 4 h of hypoxia, suggesting future time-course studies are warranted in the exploration of furry African mole-rat responses to hypoxia.

Indeed, the natural history of these species can help explain why certain mole-rats show marked changes in miRNA expression or HIF-1α protein abundance, but not others. *Bathyergus suillus* and *G. capensis* are solitary species, whereas the *Cryptomys hottentotus* subspecies are social, and *H. glaber* live in large, eusocial colonies (Bennett and Faulkes, 2000; Robb et al., 2012). Their sociality undoubtedly impacts their foraging and burrowing behaviors and, as a result, their capacity to tolerate hypoxia. *Bathyergus suillus* live in soft, sandy soils and alone; consequently, they do not dig complex tunnel systems like *C. h. hottentotus* (Thomas et al., 2009, 2013). In contrast to other mole-rats, *B. suillus* sometimes forage on the surface for grasses and forbes where O_2 is not limited, so it has less

Journal of Experimental Biology (2020) 223, jeb215905. doi:10.1242/jeb.215905

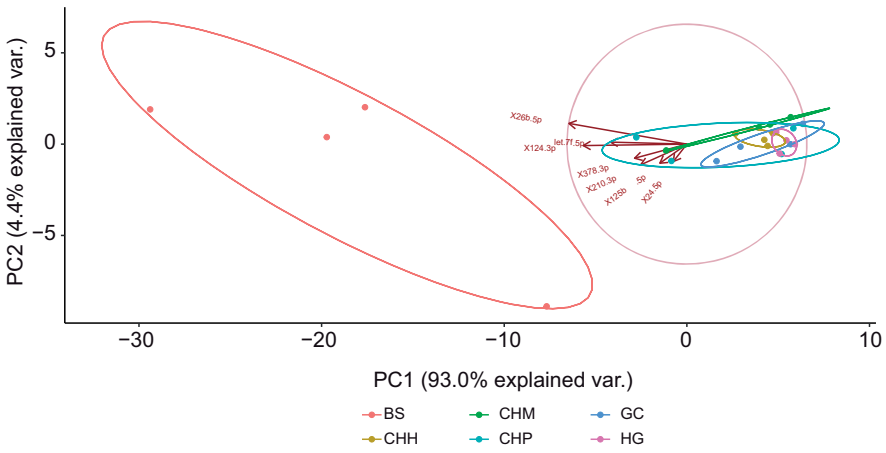

Fig. 9. PCA plot of normalized data from hypoxic groups of all species. Plot showcases the trends when only the top five contributing factors for PC1 and PC2 are considered. Species are listed as per Fig. 2.

of a need for hypoxia tolerance compared with other species of mole-rat, such as *C. h. hottentotus*, which spends 100% of its foraging time underground, searching for the underground storage organs of geophytes, in hypercapnic burrows with many other individuals. Indeed, wild-captured *B. suillus* could not withstand the same degree of hypoxia at the beginning of this experiment, nor could it reduce its metabolic rate, or change its tidal volume to compensate for changes in O_2 availability, to the same extent as the other African mole-rat species during hypoxia (Ivy et al., 2019). As a result, *B. suillus* is less hypoxia tolerant than the other species and may require more numerous and/or larger fold-changes in certain miRNAs to cope with decreases in oxygen availability. When comparing the molecular responses to hypoxia of all species (Fig. 9), *B. suillus* is statistically separate from the other species, supporting the premise that it has a unique response to hypoxia.

Specifically, to cope with low oxygen stress, *B. suillus* strongly upregulated several miRNA, including miR-26b-5p, miR-124-3p, let-7f-5p, miR-378-3p and miR-210-3p (Fig. 7). These five miRNA are noteworthy because they are the top five variables that contribute to PC1, which helps explain 92% of the differences seen between control and hypoxic brains (Fig. 8A). Each of these miRNAs has protective roles during hypoxia, and could be important for the survival of *B. suillus*, the least hypoxia-tolerant African mole-rat (Ivy et al., 2019). For instance, miR-210-3p is a hypoxia-inducible miRNA with many roles including preventing cell death and promoting tissue repair in response to ischemic and hypoxic brain damage (Meng et al., 2018; Zeng et al., 2011). Additionally, miR-210 can inhibit glycerol 3-phosphate dehydrogenase 1-like (GPD1L) expression, a protein that tags HIF for degradation (Bavelloni et al., 2017), which is consistent with elevated HIF-1α levels in brain tissue from *B. suillus*. Another miRNA that may prevent apoptosis during hypoxia in *B. suillus* is miR-378, which is reported to inhibit caspase-3 in mouse brain cells injured by ischemia (Fang et al., 2012; Zhang et al., 2016). Interestingly, hypoxia-intolerant rodents show decreased let-7f levels in their brains with hypoxia (Jeyaseelan et al., 2008), but this miRNA is strongly upregulated in hypoxic *B. suillus* brain. let-7f targets N-myc downstream-regulated gene (*NDRG3*) to inhibit angiogenesis and cell growth through the Raf-ERK pathway (Yao et al., 2017), and it may be important to upregulate it in *B. suillus* brain to maintain tissue homeostasis during hypoxia. The brain of *B. suillus* also upregulated miR-124-3p, a marker of stroke with hypoxia-inducible roles in the inhibition of autophagy, neuronal inflammation and the expression of neurodegenerative proteins such as amyloid beta and phospho-Tau (Gu et al., 2016; Leung et al., 2014; Sørensen et al., 2017). miR-124 is associated with improved neurologic outcomes and inhibition of neuroinflammation in mice after traumatic brain injury (Huang et al., 2018). Overall, increased levels of these miRNAs under hypoxic stress are likely protective against neurological damage in *B. suillus*.

The PCA plot indicates that *G. capensis* significantly increases its molecular response to hypoxia, similar to *B. suillus* (Fig. 8E). This is interesting because it is also a solitary species and occasionally forages above ground (Robb et al., 2012), suggesting that this lifestyle may be correlated with poorer hypoxia tolerance. Further, *B. suillus* and *G. capensis* have some similarities in their physiological response to hypoxia. In moderate (7–9 kPa) and severe hypoxia (3–5 kPa), both solitary species increase breathing frequency and do not suppress their metabolic rate as strongly as the more social species like *C. h. mahali* and *C. h. pretoriae* (Ivy et al., 2019). Although many molecular adaptations that *G. capensis* use are similar to those of *B. suillus*, as determined by overlap in the most important variables contributing to the principal components (Table S2), there are still differences in the response to hypoxia between *B. suillus* and the other five mole-rat species (Fig. 9). Importantly, *G. capensis* may be able to survive lower P_{O_2} than *B. suillus* and adapt to these conditions using fewer and lower fold-changes in cell signaling proteins and miRNA expression. Many of the molecular targets identified by the PCA, which explain over 75% of the variance between control and hypoxic *G. capensis* groups for PC1, were the same targets that were differentially regulated in *B. suillus* (Table S2). One of these, miR-147, was upregulated in both *G. capensis* and *B. suillus* during hypoxia. miR-147 decreases in hypoxia-treated rat adrenal medulla cells used to study cerebral ischemia, which is associated with increased apoptosis and decreased cell migration, resulting in increased Sox2 and activation of NFκB and Wnt signaling pathways (Han et al., 2017). Thus, an increase in miR-147 during hypoxia could be important to limit apoptosis in *B. suillus* and *G. capensis* brains.

If only the top five contributing factors for PC1 and PC2 are considered, there is no difference between control and hypoxic *H. glaber* groups, but if all data are considered, a difference between control and hypoxia can be detected (Fig. 8F; Fig. S2F). This suggests that *H. glaber* uses more numerous, smaller fold-changes to respond to hypoxia, rather than a few key molecular adaptations. Interestingly, the brains of *H. glaber* and *B. suillus* upregulate one or both miR-24 isomiRs while the opposite is true for *G. capensis* and *C. h. hottentotus*. Some studies implicate miR-24 in apoptosis-promoting pathways via the inhibition of anti-apoptotic XIAP (Zhou and Zhang, 2014), but decreases in miR-24 can also be

protective in ischemic rat cardiomyocytes (Li et al., 2012). Most studies identify pro-apoptotic BIM as a major miR-24 target, which means that an upregulation of miR-24 prevents apoptosis (Kulshreshtha et al., 2007; Roscigno et al., 2017; Sun et al., 2016). Therefore, an increase in miR-24 in hypoxic *H. glaber* and *B. suillus* brains would limit apoptosis. By contrast, the decrease or maintenance of this miRNA in other species could be attributed to the inherent redundancy of the miRNAome, where many different miRNAs can regulate the same process (e.g. miR-147 regulates apoptosis in *G. capensis* brain). As a result, it is important to stress that we may not have identified the main miRNAs that each species uses in response to hypoxia using the RT-qPCR method, and future studies could contribute a more thorough analysis of the miRNAome of these hypoxia-tolerant species, to identify the most important hypoxamiRs used by the brains of each species.

Lastly, all three *Cryptomys hottentotus* subspecies did not show any statistical differences between control and hypoxic groups (Fig. 8B–D), suggesting that the markers we hypothesized as being important in the hypoxic response are not the ones that these subspecies use to tolerate low oxygen or, rather, a lifestyle of foraging underground and sharing sealed burrows with other members has benefited these species by increasing their tolerance to hypoxia. Indeed, their high hypoxia tolerance may even facilitate species like *C. h. mahali* living at a range of altitudes (1600–3200 m) (Broekman et al., 2006).

Conclusion

Herein, we present species-specific hypoxia-mediated changes in HIF-1α and miRNA profiles of brains from six hypoxia-tolerant rodents. None of the mole-rat species showed evidence of protein or DNA damage during hypoxia. Furthermore, brain antioxidant capacity did not change, suggesting that all six species have sufficient antioxidant capacity to handle changes in oxygen availability. PCA analysis of all molecular data suggest that the solitary species, *B. suillus* and *G. capensis*, are the least hypoxia tolerant, requiring the highest number of miRNAs and degree of molecular regulation during hypoxic stress, whereas the least responsive species were all *C. hottentotus* subspecies. Indeed, *B. suillus* upregulated the most miRNAs during hypoxia, and most were shown to be anti-apoptotic, anti-inflammatory and anti-angiogenic. The few miRNAs that were differentially expressed in *C. h. hottentotus*, *C. h. mahali* and *H. glaber* brains were also implicated in anti-apoptotic and anti-inflammatory processes. Finally, most of the differentially expressed miRNAs in brain from *G. capensis* were implicated in suppressing apoptosis but were largely downregulated. However, the few miRNAs that did increase in response to hypoxia are postulated to have protective roles for the hypoxic brain, including inhibiting genes involved in apoptosis and neuroinflammation. These results suggest that the brain of each mole-rat species uses unique molecular mechanisms to increase hypoxia tolerance, and that *C. hottentotus* subspecies, as a result of their social and fully subterranean lifestyle, may be the most equipped to tolerate low oxygen.

Acknowledgements

We would like to thank Dr Bill Milsom and Ryan Sprenger, University of British Columbia, as well as Catherine Ivy, McMaster University, for expert help with the animal hypoxia exposures.

Competing interests

The authors declare no competing or financial interests.

Author contributions

Conceptualization: S.M.L., K.E.S., N.C.B., D.W.H., B.v.J., M.E.P., K.B.S.; Methodology: S.M.L., K.E.S., N.C.B., D.W.H., B.v.J., M.E.P., K.B.S.; Validation: S.M.L., K.E.S.; Formal analysis: S.M.L., K.E.S.; Investigation: S.M.L., K.E.S.; Resources: N.C.B., D.W.H., B.v.J., M.E.P., K.B.S.; Data curation: S.M.L., K.E.S.; Writing - original draft: S.M.L., K.E.S.; Writing - review & editing: S.M.L., K.E.S., N.C.B., D.W.H., M.E.P., K.B.S.; Visualization: S.M.L., K.E.S., N.C.B., D.W.H., B.v.J., M.E.P., K.B.S.; Supervision: K.B.S.; Project administration: N.C.B., M.E.P., K.B.S.; Funding acquisition: N.C.B., M.E.P., K.B.S.

Funding

The Storey lab acknowledges the support of a Discovery grant from the Natural Sciences and Engineering Research Council of Canada (NSERC; 6793) and an NSERC postgraduate scholarship to S.M.L. K.B.S. holds the Canada Research Chair in Molecular Physiology. The Bennett lab acknowledge support from the Department of Science and Technology, Republic of South Africa and National Research Foundation (DST-NRF; 64756). The Pamenter lab is supported by an NSERC Discovery Grant and a Natural Geographic Explorers Grant to M.E.P. M.E.P. also holds a Canada Research Chair in Comparative Neurophysiology.

Data availability

Supplementary information

Supplementary information available online at
http://jeb.biologists.org/lookup/doi/10.1242/jeb.215905.supplemental

References

Andziak, B., O'Connor, T. P. and Buffenstein, R. (2005). Antioxidants do not explain the disparate longevity between mice and the longest-living rodent, the naked mole-rat. *Mech. Ageing Dev.* **126**, 1206-1212. doi:10.1016/j.mad.2005.06.009

Andziak, B., O'Connor, T. P., Qi, W., DeWaal, E. M., Pierce, A., Chaudhuri, A. R., Van Remmen, H. and Buffenstein, R. (2006). High oxidative damage levels in the longest-living rodent, the naked mole-rat. *Aging Cell* **5**, 463-471. doi:10.1111/j.1474-9726.2006.00237.x

Ashcroft, S. J. H. and Ashcroft, F. M. (1990). Properties and functions of ATP-sensitive K-channels. *Cell. Signal.* **2**, 197-214. doi:10.1016/0898-6568(90)90048-F

Bavelloni, A., Ramazzotti, G., Poli, A., Piazzi, M., Focaccia, E., Blalock, W. and Faenza, I. (2017). MiRNA-210: a current overview. *Anticancer Res.* **37**, 6511-6521.

Bennett, N. C. (1992). The locomotory activity patterns of a functionally complete colony of *Cryptomys hottentotus hottentotus* (Rodentia: Bathyergidae). *J. Zool.* **228**, 435-443. doi:10.1111/j.1469-7998.1992.tb04446.x

Bennett, N. C. and Faulkes, C. G. (2000). *African Mole-Rats: Ecology and Eusociality*. Cambridge, UK: Cambridge University Press.

Biggar, K. K., Luu, B. E., Wu, C. W., Pifferi, F., Perret, M. and Storey, K. B. (2018). Identification of novel and conserved microRNA and their expression in the gray mouse lemur, *Microcebus murinus*, a primate capable of daily torpor. *Gene* **677**, 332-339. doi:10.1016/j.gene.2018.08.014

Broekman, M., Bennett, N. C., Jackson, C. R. and Scantlebury, M. (2006). Mole-rats from higher altitudes have greater thermoregulatory capabilities. *Physiol. Behav.* **89**, 750-754. doi:10.1016/j.physbeh.2006.08.023

Buck, L. T. and Pamenter, M. E. (2018). The hypoxia-tolerant vertebrate brain: arresting synaptic activity. *Comp. Biochem. Physiol. B Biochem. Mol. Biol.* **224**, 61-70. doi:10.1016/j.cbpb.2017.11.015

Caballero, B., Tomás-Zapico, C., Vega-Naredo, I., Sierra, V., Tolivia, D., Hardeland, R., Rodríguez-Colunga, M. J., Joel, A., Nevo, E., Avivi, A. et al. (2006). Antioxidant activity in *Spalax ehrenbergi*: a possible adaptation to underground stress. *J. Comp. Physiol. A Neuroethol. Sens. Neural Behav. Physiol.* **192**, 753-759. doi:10.1007/s00359-006-0111-z

Dalle-Donne, I., Aldini, G., Carini, M., Colombo, R., Rossi, R. Milzani, A. (2006). Protein carbonylation, cellular dysfunction, and disease progression. *J. Cell. Mol. Med.* **10**, 389-406. doi:10.1111/j.1582-4934.2006.tb00407.x

Dengler, V. L., Galbraith, M. D. and Espinosa, J. M. (2014). Transcriptional regulation by hypoxia inducible factors. *Crit. Rev. Biochem. Mol. Biol.* **49**, 1-15. doi:10.3109/10409238.2013.838205

Dunn, J. F., Grinberg, O., Roche, M., Nwaigwe, C. I., Hou, H. G. and Swartz, H. M. (2000). Noninvasive assessment of cerebral oxygenation during acclimation to hypobaric hypoxia. *J. Cereb. Blood Flow Metab.* **20**, 1632-1635. doi:10.1097/00004647-200012000-00002

Evdokimov, A., Kutuzov, M., Petruseva, I., Lukjanchikova, N., Kashina, E., Kolova, E., Zemerova, T., Romanenko, S., Perelman, P., Prokopov, D. et al. (2018). Naked mole rat cells display more efficient excision repair than mouse cells. *Aging* **10**, 1454-1473. doi:10.18632/aging.101482

Fang, J., Song, X.-W., Tian, J., Chen, H.-Y., Li, D.-F., Wang, J.-F., Ren, A.-J., Yuan, W.-J. and Lin, L. (2012). Overexpression of microRNA-378 attenuates ischemia-induced apoptosis by inhibiting caspase-3 expression in cardiac myocytes. *Apoptosis* **17**, 410-423. doi:10.1007/s10495-011-0683-0

Fang, X., Seim, I., Huang, Z., Gerashchenko, M. V., Xiong, Z., Turanov, A. A., Zhu, Y., Lobanov, A. V., Fan, D., Yim, S. H. et al. (2014). Adaptations to a

subterranean environment and longevity revealed by the analysis of mole rat genomes. *Cell Repair* **8**, 1354-1364. doi:10.1016/j.celrep.2014.07.030

Faulkes, C. G., Verheyen, E., Verheyen, W., Jarvis, J. U. M. and Bennett, N. C. (2004). Phylogeographical patterns of genetic divergence and speciation in African mole-rats (Family: *Bathyergidae*). *Mol. Ecol.* **13**, 613-629. doi:10.1046/j.1365-294X.2004.02099.x

Folbergrová, J., Minamisawa, H., Ekholm, A. and Siesjö, B. K. (1990). Phosphorylase a and labile metabolites during anoxia: correlation to membrane fluxes of K+ and Ca2+. *J. Neurochem.* **55**, 1690-1696. doi:10.1111/j.1471-4159.1990.tb04957.x

Garbarino, V. R., Orr, M. E., Rodriguez, K. A. and Buffenstein, R. (2015). Mechanisms of oxidative stress resistance in the brain: lessons learned from hypoxia tolerant extremophilic vertebrates. *Arch. Biochem. Biophys.* **576**, 8-16. doi:10.1016/j.abb.2015.01.029

Gu, H., Liu, M., Ding, C., Wang, X., Wang, R., Wu, X. and Fan, R. (2016). Hypoxia-responsive miR-124 and miR-144 reduce hypoxia-induced autophagy and enhance radiosensitivity of prostate cancer cells via suppressing PIM1. *Cancer Med.* **5**, 1174-1182. doi:10.1002/cam4.664

Han, L., Dong, Z., Liu, N., Xie, F. and Wang, N. (2017). Maternally expressed gene 3 (MEG3) enhances PC12 cell hypoxia injury by targeting miR-147. *Cell. Physiol. Biochem.* **43**, 2457-2469. doi:10.1159/000484452

Holmes, M. M., Goldman, B. D., Goldman, S. L., Seney, M. L. and Forger, N. G. (2009). Neuroendocrinology and sexual differentiation in eusocial mammals. *Front. Neuroendocrinol.* **30**, 519-533. doi:10.1016/j.yfrne.2009.04.010

Huang, S., Ge, X., Yu, J., Han, Z., Yin, Z., Li, Y., Chen, F., Wang, H., Zhang, J. and Lei, P. (2018). Increased miR-124-3p in microglial exosomes following traumatic brain injury inhibits neuronal inflammation and contributes to neurite outgrowth via their transfer into neurons. *FASEB J.* **32**, 512-528. doi:10.1096/fj.201700673R

Ingram, C. M., Burda, H. and Honeycutt, R. L. (2004). Molecular phylogenetics and taxonomy of the African mole-rats, genus *Cryptomys* and the new genus *Coetomys Gray*, 1864. *Mol. Phylogenet. Evol.* **31**, 997-1014. doi:10.1016/j.ympev.2003.11.004

Ivy, C. M., Sprenger, R. J., Bennett, N. C., van Jaarsveld, B., Hart, D. W., Kirby, A. M., Yaghoubi, D., Storey, K. B., Milsom, W. K. and Pamenter, M. E. (2020). The Hypoxia Tolerance of Eight Related African Mole-Rat Species Rivals That of Naked Mole-Rats, Despite Divergent Ventilatory and Metabolic Strategies in Severe Hypoxia. *Acta Physiol.* **228**, e13436. doi: 10.1111/apha.13436

Jarvis, J. (1981). Eusociality in a mammal: cooperative breeding in naked mole-rat colonies. *Science* **212**, 571-573. doi:10.1126/science.7209555

Jeyaseelan, K., Lim, K. Y. and Armugam, A. (2008). MicroRNA expression in the blood and brain of rats subjected to transient focal ischemia by middle cerebral artery occlusion. *Stroke* **39**, 959-966. doi:10.1161/STROKEAHA.107.500736

Johansen, K., Lykkeboe, G., Weber, R. E. and Maloiy, G. M. O. (1976). Blood respiratory properties in the naked mole rat *Heterocephalus glaber*, a mammal of low body temperature. *Respir. Physiol.* **28**, 303-314. doi:10.1016/0034-5687(76)90025-6

Josse, J. and Husson, F. (2016). missMDA: a package for handling missing values in multivariate data analysis. *J. Stat. Softw.* **70**. doi:10.18637/jss.v070.i01

Kim, E. B., Fang, X., Fushan, A. A., Huang, Z., Lobanov, A. V., Han, L., Marino, S. M., Sun, X., Turanov, A. A., Yang, P. et al. (2011). Genome sequencing reveals insights into physiology and longevity of the naked mole rat. *Nature* **479**, 223-227. doi:10.1038/nature10533

Kulshreshtha, R., Ferracin, M., Wojcik, S. E., Garzon, R., Alder, H., Agosto-Perez, F. J., Davuluri, R., Liu, C.-G., Croce, C. M., Negrini, M. et al. (2007). A microRNA signature of hypoxia. *Mol. Cell. Biol.* **27**, 1859-1867. doi:10.1128/MCB.01395-06

Larson, J. and Park, T. J. (2009). Extreme hypoxia tolerance of naked mole-rat brain. *Neuroreport* **20**, 1634-1637. doi:10.1097/WNR.0b013e32833370cf

Leung, L. Y., Chan, C. P. Y., Leung, Y. K., Jiang, H. L., Abrigo, J. M., Wang, D. F., Chung, J. S. H., Rainer, T. H. and Graham, C. A. (2014). Comparison of miR-124-3p and miR-16 for early diagnosis of hemorrhagic and ischemic stroke. *Clin. Chim. Acta* **433**, 139-144. doi:10.1016/j.cca.2014.03.007

Li, D. F., Tian, J., Guo, X., Huang, L. M., Xu, Y., Wang, C. C., Wang, J. F., Ren, A. J., Yuan, W. J. and Lin, L. (2012). Induction of microRNA-24 by HIF-1 protects against ischemic injury in rat cardiomyocytes. *Physiol. Res.* **61**, 555-565.

Macrae, S. L., Zhang, Q., Lemetre, C., Seim, I., Calder, R. B., Hoeijmakers, J., Suh, Y., Gladyshev, V. N., Seluanov, A., Gorbunova, V. et al. (2015). Comparative analysis of genome maintenance genes in naked mole rat, mouse, and human. *Aging Cell* **14**, 288-291. doi:10.1111/acel.12314

McNab, B. K. (1966). The metabolism of fossorial rodents: a study of convergence. *Ecology* **47**, 712-733. doi:10.2307/1934259

Meng, Z.-Y., Kang, H.-L., Duan, W., Zheng, J., Li, Q.-N. and Zhou, Z.-J. (2018). MicroRNA-210 promotes accumulation of neural precursor cells around ischemic foci after cerebral ischemia by regulating the SOCS1–STAT3–VEGF-C pathway. *J. Am. Heart Assoc.* **7**, e005052. doi:10.1161/JAHA.116.005052

Mirtschink, P. and Krek, W. (2016). Hypoxia-driven glycolytic and fructolytic metabolic programs: pivotal to hypertrophic heart disease. *Biochim. Biophys. Acta Mol. Cell Res.* **1863**, 1822-1828. doi:10.1016/j.bbamcr.2016.02.011

Munro, D., Baldy, C., Pamenter, M. E. and Treberg, J. R. (2019). The exceptional longevity of the naked mole-rat may be explained by mitochondrial antioxidant defenses. *Aging Cell* **18**, e12916. doi:10.1111/acel.12916

Nair, D., Ramesh, V. and Gozal, D. (2012). Adverse cognitive effects of high-fat diet in a murine model of sleep apnea are mediated by NADPH oxidase activity. *Neuroscience* **227**, 361-369. doi:10.1016/j.neuroscience.2012.09.068

Nakajima, H. (2012). The relation of urinary 8-OHdG, a marker of oxidative stress to DNA, and clinical outcomes for ischemic stroke. *Open Neurol. J.* **6**, 51-57. doi:10.2174/1874205X01206010051

Nortje, J. and Gupta, A. K. (2006). The role of tissue oxygen monitoring in patients with acute brain injury. *Br. J. Anaesth.* **97**, 95-106. doi:10.1093/bja/ael137

Pamenter, M. E., Dzal, Y. A. and Milsom, W. K. (2015). Adenosine receptors mediate the hypoxic ventilatory response but not the hypoxic metabolic response in the naked mole rat during acute hypoxia. *Proc. Biol. Sci.* **282**, 20141722. doi:10.1098/rspb.2014.1722

Pamenter, M. E., Lau, G. Y., Richards, J. G. and Milsom, W. K. (2018). Naked mole rat brain mitochondria electron transport system flux and H^+ leak are reduced during acute hypoxia. *J. Exp. Biol.* **221**, jeb171397. doi:10.1242/jeb.171397

Papandreou, I., Cairns, R. A., Fontana, L., Lim, A. L. and Denko, N. C. (2006). HIF-1 mediates adaptation to hypoxia by actively downregulating mitochondrial oxygen consumption. *Cell Metab.* **3**, 187-197. doi:10.1016/j.cmet.2006.01.012

Park, T. J., Reznick, J., Peterson, B. L., Blass, G., Omerbašić, D., Bennett, N. C., Kuich, P. H. J. L., Zasada, C., Browe, B. M., Hamann, W. et al. (2017). Fructose-driven glycolysis supports anoxia resistance in the naked mole-rat. *Science* **356**, 307-311. doi:10.1126/science.aab3896

Perez, V. I., Buffenstein, R., Masamsetti, V., Leonard, S., Salmon, A. B., Mele, J., Andziak, B., Yang, T., Edrey, Y., Friguet, B. et al. (2009). Protein stability and resistance to oxidative stress are determinants of longevity in the longest-living rodent, the naked mole-rat. *Proc. Natl. Acad. Sci. USA* **106**, 3059-3064. doi:10.1073/pnas.0809620106

Robb, G. N., Woodborne, S. and Bennett, N. C. (2012). Subterranean sympatry: an investigation into diet using stable isotope analysis. *PLoS ONE* **7**. doi:10.1371/journal.pone.0048572

Rolett, E. L., Azzawi, A., Liu, K. J., Yongbi, M. N., Swartz, H. M. and Dunn, J. F. (2000). Critical oxygen tension in rat brain: a combined 31 P-NMR and EPR oximetry study. *Am. J. Physiol. Integr. Comp. Physiol.* **279**, R9-R16. doi:10.1152/ajpregu.2000.279.1.R9

Roscigno, G., Puoti, I., Giordano, I., Donnarumma, E., Russo, V., Affinito, A., Adamo, A., Quintavalle, C., Todaro, M., Vivanco, M. D. M. et al. (2017). MiR-24 induces chemotherapy resistance and hypoxic advantage in breast cancer. *Oncotarget* **8**, 19507-19521. doi:10.18632/oncotarget.14470

Schmidt, H., Hangmann, J., Shams, I., Avivi, A. and Hankeln, T. (2016). Molecular evolution of antioxidant and hypoxia response in long-lived, cancer-resistant blind mole rats: the Nrf2-Keap1 pathway. *Gene* **577**, 293-298. doi:10.1016/j.gene.2015.11.038

Schülke, S., Dreidax, D., Malik, A., Burmester, T., Nevo, E., Band, M., Avivi, A. and Hankeln, T. (2012). Living with stress: regulation of antioxidant defense genes in the subterranean, hypoxia-tolerant mole rat, *Spalax*. *Gene* **500**, 199-206. doi:10.1016/j.gene.2012.03.019

Shams, I., Avivi, A. and Nevo, E. (2004). Hypoxic stress tolerance of the blind subterranean mole rat: expression of erythropoietin and hypoxia-inducible factor 1α. *Proc. Natl. Acad. Sci. USA* **101**, 9698-9703. doi:10.1073/pnas.0403540101

Shams, I., Malik, A., Manov, I., Joel, A., Band, M. and Avivi, A. (2013). Transcription pattern of p53-targeted DNA repair genes in the hypoxia-tolerant subterranean mole rat *Spalax*. *J. Mol. Biol.* **425**, 1111-1118. doi:10.1016/j.jmb.2013.01.007

Smith, K. A., Waypa, G. B. and Schumacker, P. T. (2017). Redox signaling during hypoxia in mammalian cells. *Redox Biol.* **13**, 228-234. doi:10.1016/j.redox.2017.05.020

Sørensen, S. S., Nygaard, A.-B., Carlsen, A. L., Heegaard, N. H. H., Bak, M. and Christensen, T. (2017). Elevation of brain-enriched miRNAs in cerebrospinal fluid of patients with acute ischemic stroke. *Biomark. Res.* **5**, 24. doi:10.1186/s40364-017-0104-9

Sun, X., Ren, Z., Pan, Y. and Zhang, C. (2016). Antihypoxic effect of miR-24 in SH-SY5Y cells under hypoxia via downregulating expression of neurocan. *Biochem. Biophys. Res. Commun.* **477**, 692-699. doi:10.1016/j.bbrc.2016.06.121

Terraneo, L., Paroni, R., Bianciardi, P., Giallongo, T., Carelli, S., Gorio, A. and Samaja, M. (2017). Brain adaptation to hypoxia and hyperoxia in mice. *Redox Biol.* **11**, 12-20. doi:10.1016/j.redox.2016.10.018

Thomas, H. G., Bateman, P. W., Le Comber, S. C., Bennett, N. C., Elwood, R. W. and Scantlebury, M. (2009). Burrow architecture and digging activity in the Cape dune mole rat. *J. Zool.* **279**, 277-284. doi:10.1111/j.1469-7998.2009.00616.x

Thomas, H. G., Scantlebury, M., Swanepoel, D., Bateman, P. W. and Bennett, N. C. (2013). Seasonal changes in burrow geometry of the common mole rat (Rodentia: Bathyergidae). *Naturwissenschaften* **100**, 1023-1030. doi:10.1007/s00114-013-1105-7

Tregub, P. P., Kulikov, V. P., Bespalov, A. G., Vvedensky, A. J. and Osipov, I. S. (2013). Neuroprotective effects of individual or combined exposure to hypoxia and hypercapnia in the experiment. *Bull. Exp. Biol. Med.* **155**, 327-329. doi:10.1007/s10517-013-2145-x

Truettner, J. S., Katyshev, V., Esen-Bilgin, N., Dietrich, W. D. and Dore-Duffy, P. (2013). Hypoxia alters microRNA expression in rat cortical pericytes. *MicroRNA* **2**, 32-45. doi:10.2174/2211536611302010005

Veasey, S. C., Davis, C. W., Fenik, P., Zhan, G., Hsu, Y.-J., Pratico, D. and Gow, A. (2004). Long-term intermittent hypoxia in mice: protracted hypersomnolence with oxidative injury to sleep-wake brain regions. *Sleep* **27**, 194-201. doi:10.1093/sleep/27.2.194

Willmore, W. G. and Storey, K. B. (1997). Antioxidant systems and anoxia tolerance in a freshwater turtle *Trachemys scripta elegans*. *Mol. Cell. Biochem.* **170**, 177-185. doi:10.1023/A:1006817806010

Xiao, B., Wang, S., Yang, G., Sun, X., Zhao, S., Lin, L., Cheng, J., Yang, W., Cong, W., Sun, W. et al. (2017). HIF-1α contributes to hypoxia adaptation of the naked mole rat. *Oncotarget* **8**, 109941-109951. doi:10.18632/oncotarget.22767

Yao, Y., Wang, W., Jing, L., Wang, Y., Li, M., Hou, X., Wang, J., Peng, T., Teng, J. and Jia, Y. (2017). Let-7f regulates the hypoxic response in cerebral ischemia by targeting NDRG3. *Neurochem. Res.* **42**, 446-454. doi:10.1007/s11064-016-2091-x

Zeng, L., Liu, J., Wang, Y., Wang, L., Weng, S., Tang, Y., Zheng, C., Cheng, Q., Chen, S. and Yang, G.-Y. (2011). MicroRNA-210 as a novel blood biomarker in acute cerebral ischemia. *Front. Biosci.* **3**, 1265-1272. doi:10.2741/330

Zhang, J. and Storey, K. B. (2016). RBioplot: an easy-to-use R pipeline for automated statistical analysis and data visualization in molecular biology and biochemistry. *PeerJ* **4**, e2436. doi:10.7717/peerj.2436

Zhang, N., Zhong, J., Han, S., Li, Y., Yin, Y. and Li, J. (2016). MicroRNA-378 alleviates cerebral ischemic injury by negatively regulating apoptosis executioner caspase-3. *Int. J. Mol. Sci.* **17**, 1427. doi:10.3390/ijms17091427

Zhou, J. and Zhang, J. (2014). Identification of miRNA-21 and miRNA-24 in plasma as potential early stage markers of acute cerebral infarction. *Mol. Med. Rep.* **10**, 971-976. doi:10.3892/mmr.2014.2245

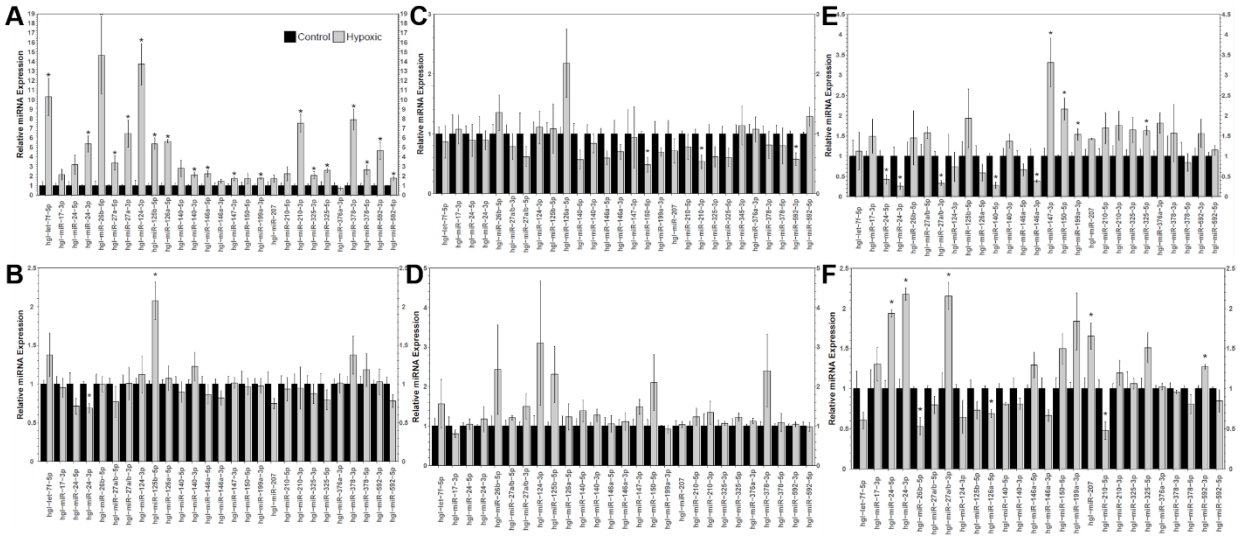

Figure S1: Relative miRNA expression levels in (A) *Bathyergus suillus*, (B) *Cryptomys hottentotus hottentotus*, (C) *Cryptomys hottentotus mahali*, (D) *Cryptomys hottentotus pretoriae*, (E) *Georychus capensis*, and (F) *Heterocephalus glaber* brain tissue in response to hypoxia. Data are mean ± SEM, $n = 4$ RNA isolations from different individuals for each species. *Asterisks* indicate data that are significantly different from the control condition ($p < 0.05$).

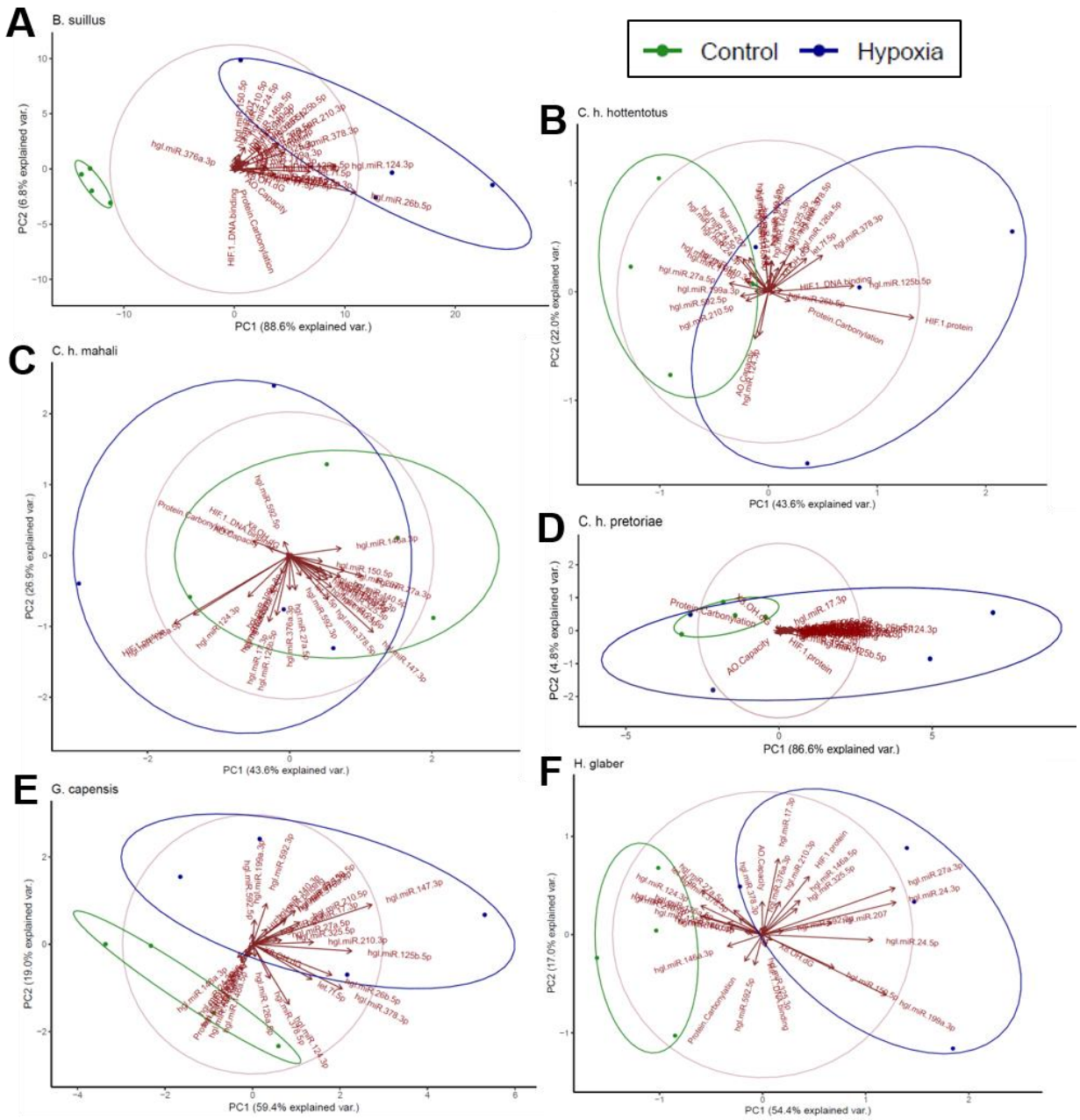

Figure S2. Principal component analysis (PCA) of the molecular data from each individual mole-rat species. PCA plots A-F show how normalized data from control (green ellipse) and hypoxic (blue ellipse) groups cluster when considering all molecular data.

Table S1: MiRNA sequences and forward primers designed from *Heterocephalus glaber* (hgl).

miRNA	Mature sequence (5' - 3')	Primer (5' - 3')
hgl-let-7f-5p	UGAGGUAGUAGAUUGUAUAGUU	ACACTCCAGCTGGGTGAGGTAGTAGATTG
hgl-miR-17-3p	ACUGCAGUGAGGGCACUUGUAG	ACACTCCAGCTGGGCTGCAGTGAGGGCAC
hgl-miR-24-5p	UGCCUACUGAGCUGAUAUCAGU	ACACTCCAGCTGGGTGCCTACTGAGCTGA
hgl-miR-24-3p	GGCUCAGUUCAGCAGGAACAG	ACACTCCAGCTGGGGGCTCAGTTCAGCAG
hgl-miR-26b-5p	UUCAAGUAAUUCAGGAUAGGU	ACACTCCAGCTGGGTTCAAGTAATTCAGG
hgl-miR-27a-5p	AGGGCUUAGCUGCUUGUGAGCA	ACACTCCAGCTGGGAGGGCTTAGCTGCTT
hgl-miR-27a-3p	UUCACAGUGGCUAAGUUCCGC	ACACTCCAGCTGGGTTCACAGTGGCTAAG
hgl-miR-124-3p	UAAGGCACGCGGUGAAUGCC	ACACTCCAGCTGGGTAAGGCACGCGGTGA
hgl-miR-125b-5p	UCCCUGAGACCCUAACUUGUGA	ACACTCCAGCTGGGTCCCTGAGACCCTAA
hgl-miR-126a-5p	CAUUAUUACUUUUGGUACGCG	ACACTCCAGCTGGGCATTATTACTTTTGG
hgl-miR-140-5p	CAGUGGUUUUACCCUAUGGUAG	ACACTCCAGCTGGGTGGTTTTACCCTATG
hgl-miR-140-3p	UACCACAGGGUAGAACCACGG	ACACTCCAGCTGGGACCACAGGGAAGAAC
hgl-miR-146a-5p	UGAGAACUGAAUUCCAUGGGUU	ACACTCCAGCTGGGTGAGAACTGAATTCC
hgl-miR-146a-3p	CCUGUGAAAUUCAGUUCUUCAG	ACACTCCAGCTGGGCCTGTGAAATTCAGT
hgl-miR-147-3p	GUGUGCGGAAAUGCUUCUGCUA	ACACTCCAGCTGGGGTGTGCGGAAGTGCT
hgl-miR-150-5p	UCUCCCAACCCUUGUACCAGUG	ACACTCCAGCTGGGTCTCCCAACCCCTGT
hgl-miR-199a-3p	ACAGUAGUCUGCACAUUGGUUA	ACACTCCAGCTGGGACAGTAGTCTGCACA
hgl-miR-207	GCUUCUCCUGGCUCUCCUCCCUC	ACACTCCAGCTGGGTCTCCTGTCTCTCCT
hgl-miR-210-5p	AGCCACUGCCCACCGCACACUG	ACACTCCAGCTGGGCCACTGCCCACCGCA
hgl-miR-210-3p	CUGUGCGUGUGACAGCGGCUGA	ACACTCCAGCTGGGCTGTGCGTGTGACAG
hgl-miR-325-3p	UUUAUUGAGCACCUCCUAUCAA	ACACTCCAGCTGGGTTTATTGAGCACCTA
hgl-miR-325-5p	CCUAGUAGGUGCUCAGUAAGUGU	ACACTCCAGCTGGGTAGTAGGTGCTCAGT
hgl-miR-376a-3p	AUCGUAGAGGAAAAUCCACGU	ACACTCCAGCTGGGATCGTAGAGGAAAAT
hgl-miR-378-3p	ACUGGACUUGGAGUCAGAAGG	ACACTCCAGCTGGGACTGGACTTGGAGTC
hgl-miR-378-5p	CUCCUGACUCCAGGUCCUGUGU	ACACTCCAGCTGGGCTCCTGACTCCAGGT
hgl-miR-592-3p	UCAUCACGUGGUGACGCAACAU	ACACTCCAGCTGGGATCACGTGGTGACGC
hgl-miR-592-5p	AUUGUGUCAAUAUGCGAUGAUGU	ACACTCCAGCTGGGATTGTGTCAATATGC

Table S2: List of top 5 contributing factors to PC1 and PC2 for each species using the data from control and hypoxic animals and then considering all species together using only the data from hypoxic groups. Variables that are not bolded were repeats of the variables used for PCA plots (bolded). For C. h. pretoriae, there were only three variables that appeared above the reference line of the barplots generated by the fviz_contrib function, indicating only three variables contribute to PC2 in this species.

Species	***Top 5 variables contributing to PC1***	***Top 5 variables contributing to PC2***
B. suillus	**26b-5p, 124-3p let-7f-5p, 378-3p, 210-3p**	210-3p, 26b-5p, **24-5p**, **125b-5p**, 378-3p
C. h. hottentotus	**HIF1 protein, 125b-5p, 378-3p, 27a-5p, let-7f-5p**	**AO capacity, 378-5p**, **124-3p**, **325-5p,** 378-3p
C. h. mahali	**HIF1 protein, 126a-5p, 147-3p, 27a-3p, 207**	147-3p, HIF1 protein, **17-3p, 125-5p**, 126a-5p
C. h. pretoriae	**124-3p, 26b-5p, 378-3p, 150-5p, let-7f-5p**	**125b-5p**, 26b-5p, **17-3p**
G. capensis	**147-3p, 125b-5p, 378-3p, 26b-5p, 210-3p**	**124-3p**, 378-3p, **592-3p,** 147-3p, **let-7f-5p**
H. glaber	**24-3p, 27a-3p, 199a-3p, 24-5p, 150-5p**	**17-3p**, 199a-3p, **HIF1 protein,** 27a-3p, **let-7f**
All species	**26b-5p, 124-3p let-7f-5p, 378-3p, 210-3p**	210-3p, **24-5p,** 26b-5p, **125b-5p**, 378-3p

Table S3: General functions of miRNAs implicated in the response to hypoxia in the brains of several species of mole-rats.

miRNA	Function	Reference(s)
	Apoptosis	
miR-24	Inhibit apoptosis and HIF degradation	(Roscigno et al., 2017; Sun et al., 2016)
miR-27	Inhibit apoptosis	(Chen et al., 2014; Sabirzhanov et al., 2014)
miR-26 (decrease)	Anti-apoptosis, anti-autophagy	(Nallamshetty et al., 2013)
miR-147	Inhibit apoptosis	(Han et al., 2017)
miR-207	Anti-apoptosis, anti-autophagy	(Tao et al., 2015)
miR-210	Anti-apoptosis, pro-angiogenesis and tissue repair Inhibit HIF degradation	(Meng et al., 2018; Zeng et al., 2011) (Bavelloni et al., 2017)
miR-378	Inhibit apoptosis	(Fang et al., 2012)
miR-592	Inhibit apoptosis Cell proliferation, Cellular metabolism Inhibits astrogliogenesis differentiation and cell maturation	(Irmady et al., 2014) (He et al., 2018) (Haque et al., 2016; Jia et al., 2016) (Zhang et al., 2013)
	Inflammation	
miR-124	Inhibit neuroinflammation Suppresses autophagy	(Huang et al., 2018) (Gu et al., 2016)
miR-125b	Pro-inflammatory Neuroprotective – promote neuronal lipid membranes Promotes neuronal differentiation	(Mar-Aguilar et al., 2013; Rink and Khanna, 2011; Zhang et al., 2017) (Zhang et al., 2019) (Xiu et al., 2018)
miR-140	Enhance cerebral protection	(Han et al., 2018; Truettner et al., 2013)
miR-146	5p isomer inhibits inflammation via NFkB 3p isomir increases pro-inflammatory IL-8	(Li et al., 2017; Nallamshetty et al., 2013) (Gysler et al., 2016)
miR-150	Inhibit cell proliferation and migration during stress via HIF and regulates inflammation	(Truettner et al., 2013)
miR-210	Anti-inflammatory via targeting NFκB	(Li et al., 2017)
	Circadian Rhythms	
miR-325	Circadian rhythm – melatonin synthesis	(Yang et al., 2017)
	Angiogenesis	
miR-let-7f	Inhibits angiogenesis through Raf-ERK	(Yao et al., 2017)
miR-126	Inhibits angiogenesis Involved in vascular integrity and cell function	(Mishra et al., 2009)
miR-199	Inhibits angiogenesis through HIF-1/VEGF	(Dai et al., 2015)

References

Bavelloni, A., Ramazzotti, G., Poli, A., Piazzi, M., Focaccia, E., Blalock, W. and Faenza, I. (2017). MiRNA-210: a current overview. *Anticancer Res* **37**, 6511–6521.

Chen, Q., Xu, J., Li, L., Li, H., Mao, S., Zhang, F., Zen, K., Zhang, C. Y. and Zhang, Q. (2014). MicroRNA-23a/b and microRNA-27a/b suppress Apaf-1 protein and alleviate hypoxia-induced neuronal apoptosis. *Cell Death Dis.* **5**, 1–12.

Dai, L., Lou, W., Zhu, J., Zhou, X. and Di, W. (2015). MiR-199a inhibits the angiogenic potential of endometrial stromal cells under hypoxia by targeting HIF-1α/VEGF pathway. *Int J Clin Exp Pathol* **8**, 4735–4744.

Fang, J., Song, X.-W., Tian, J., Chen, H.-Y., Li, D.-F., Wang, J.-F., Ren, A.-J., Yuan, W.-J. and Lin, L. (2012). Overexpression of microRNA-378 attenuates ischemia-induced apoptosis by inhibiting caspase-3 expression in cardiac myocytes. *Apoptosis* **17**, 410–423.

Gu, H., Liu, M., Ding, C., Wang, X., Wang, R., Wu, X. and Fan, R. (2016). Hypoxia-responsive miR-124 and miR-144 reduce hypoxia-induced autophagy and enhance radiosensitivity of prostate cancer cells via suppressing PIM1. *Cancer Med.* **5**, 1174–1182.

Gysler, S. M., Mulla, M. J., Guerra, M., Brosens, J. J., Salmon, J. E., Chamley, L. W. and Abrahams, V. M. (2016). Antiphospholipid antibody-induced miR-146a-3p drives trophoblast interleukin-8 secretion through activation of Toll-like receptor 8. *Mol. Hum. Reprod.* **22**, 465–474.

Han, L., Dong, Z., Liu, N., Xie, F. and Wang, N. (2017). Maternally expressed gene 3 (MEG3) enhances PC12 cell hypoxia injury by targeting miR-147. *Cell. Physiol. Biochem.* **43**, 2457–2469.

Han, X.-R., Wen, X., Wang, Y.-J., Wang, S., Shen, M., Zhang, Z.-F., Fan, S.-H., Shan, Q., Wang, L., Li, M.-Q., et al. (2018). MicroRNA-140-5p elevates cerebral protection of dexmedetomidine against hypoxic-ischaemic brain damage via the Wnt/β-catenin signalling pathway. *J. Cell. Mol. Med.* **22**, 3167–3182.

Haque, M., Kendal, J. K., MacIsaac, R. M. and Demetrick, D. J. (2016). WSB1: from homeostasis to hypoxia. *J. Biomed. Sci.* **23**, 61.

He, Y., Ge, Y., Jiang, M., Zhou, J., Luo, D., Fan, H., Shi, L., Lin, L. and Yang, L. (2018). MiR-592 promotes gastric cancer proliferation, migration, and invasion through the PI3K/AKT and MAPK/ERK signaling pathways by targeting Spry2. *Cell. Physiol. Biochem.* **47**, 1465–1481.

Huang, S., Ge, X., Yu, J., Han, Z., Yin, Z., Li, Y., Chen, F., Wang, H., Zhang, J. and Lei, P. (2018). Increased miR-124-3p in microglial exosomes following traumatic brain injury inhibits neuronal inflammation and contributes to neurite outgrowth via their transfer into neurons. *FASEB J.* **32**, 512–528.

Irmady, K., Jackman, K. A., Padow, V. A., Shahani, N., Martin, L. A., Cerchietti, L., Unsicker, K., Iadecola, C. and Hempstead, B. L. (2014). MiR-592 regulates the induction and cell death-promoting activity of p75NTR in neuronal ischemic injury. *J. Neurosci.* **34**, 3419–3428.

Jia, Y.-Y., Zhao, J.-Y., Li, B.-L., Gao, K., Song, Y., Liu, M.-Y., Yang, X.-J., Xue, Y., Wen, A.-D. and Shi, L. (2016). miR-592/WSB1/HIF-1alpha axis inhibits glycolytic metabolism to decrease hepatocellular carcinoma growth. *Oncotarget* **7**,.

Li, B., Concepcion, K., Meng, X. and Zhang, L. (2017). Brain-immune interactions in perinatal hypoxic-ischemic brain injury. *Prog. Neurobiol.* **159**, 50–68.

Mar-Aguilar, F., Luna-Aguirre, C. M., Moreno-Rocha, J. C., Araiza-Chavez, J., Trevino, V., Rodriguez-Padilla, C. and Resendez-Perez, D. (2013). Differential expression of miR-21, miR-125b and miR-191 in breast cancer tissue. *Asia. Pac. J. Clin. Oncol.* **9**, 53–59.

Meng, Z., Kang, H., Duan, W., Zheng, J., Li, Q. and Zhou, Z. (2018). MicroRNA- 210 promotes accumulation of neural precursor cells around ischemic foci after cerebral ischemia by regulating the SOCS1–STAT3–VEGF- C pathway. *J. Am. Heart Assoc.* **7**,.

Mishra, P. K., Tyagi, N., Kumar, M. and Tyagi, S. C. (2009). MicroRNAs as a therapeutic target for cardiovascular diseases. *J. Cell. Mol. Med.* **13**, 778–789.

Nallamshetty, S., Chan, S. Y. and Loscalzo, J. (2013). Hypoxia: A master regulator of microRNA biogenesis and activity. *Free Radic. Biol. Med.* **64**, 20–30.

Rink, C. and Khanna, S. (2011). MicroRNA in ischemic stroke etiology and pathology. *Physiol. Genomics* **43**, 521–528.

Roscigno, G., Puoti, I., Giordano, I., Donnarumma, E., Russo, V., Affinito, A., Adamo, A., Quintavalle, C., Todaro, M., dM Vivanco, M., et al. (2017). MiR-24 induces chemotherapy resistance and hypoxic advantage in breast cancer. *Oncotarget* **8**, 19507–19521.

Sabirzhanov, B., Zhao, Z., Stoica, B. A., Loane, D. J., Wu, J., Borroto, C., Dorsey, S. G. and Faden, A. I. (2014). Downregulation of miR-23a and miR-27a following experimental traumatic brain injury induces neuronal cell death through activation of proapoptotic Bcl-2 proteins. *J. Neurosci.* **34**, 10055–10071.

Sun, X., Ren, Z., Pan, Y. and Zhang, C. (2016). Antihypoxic effect of miR-24 in SH-SY5Y cells under hypoxia via downregulating expression of neurocan. *Biochem. Biophys. Res. Commun.* **477**, 692–699.

Tao, J., Liu, W., Shang, G., Zheng, Y., Huang, J., Lin, R. and Chen, L. (2015). MiR-207/352 regulate lysosomal-associated membrane proteins and enzymes following ischemic stroke. *Neuroscience* **305**, 1–14.

Truettner, J. S., Katyshev, V., Esen-Bilgin, N., Dietrich, W. D. and Dore-Duffy, P. (2013). Hypoxia alters microRNA expression in rat cortical pericytes. *MicroRNA* **2**, 32–45.

Xiu, L., Xing, Q., Mao, J., Sun, H., Teng, W. and Shan, Z. (2018). miRNA-125b-5p suppresses hypothyroidism development by targeting signal transducer and activator of transcription 3. *Med. Sci. Monit.* **24**, 5041–5049.

Yang, Y., Sun, B., Huang, J., Xu, L., Pan, J., Fang, C., Li, M., Li, G., Tao, Y., Yang, X., et al. (2017). Up-regulation of miR-325-3p suppresses pineal aralkylamine N-acetyltransferase (Aanat) after neonatal hypoxia–ischemia brain injury in rats. *Brain Res.* **1668**, 28–35.

Yao, Y., Wang, W., Jing, L., Wang, Y., Li, M., Hou, X., Wang, J., Peng, T., Teng, J. and Jia, Y. (2017). Let-7f regulates the hypoxic response in cerebral ischemia by targeting NDRG3. *Neurochem. Res.* **42**, 446–454.

Zeng, L., Liu, J., Wang, Y., Wang, L., Weng, S., Tang, Y., Zheng, C., Cheng, Q., Chen, S. and Yang, G. Y. (2011). MicroRNA-210 as a novel blood biomarker in acute cerebral ischemia. *Front Biosci (Elite Ed)* **3**, 1265–1272.

Zhang, J., Zhang, J., Zhou, Y., Wu, Y.-J., Ma, L., Wang, R.-J., Huang, S.-Q., Gao, R.-R., Liu, L.-H., Shao, Z.-H., et al. (2013). Novel cerebellum-enriched miR-592 may play a role in neural progenitor cell differentiation and neuronal maturation through regulating Lrrc4c and Nfasc in rat. *Curr. Mol. Med.* **13**, 1432–45.

Zhang, B., Wang, L.-S. and Zhou, Y.-H. (2017). Elevated microRNA-125b promotes inflammation in rheumatoid arthritis by activation of NF-κB pathway. *Biomed. Pharmacother.* **93**, 1151–1157.

Zhang, L., Dong, H., Si, Y., Wu, N., Cao, H., Mei, B. and Meng, B. (2019). miR-125b promotes tau phosphorylation by targeting the neural cell adhesion molecule in neuropathological progression. *Neurobiol. Aging* **73**, 41–49.